Available online at www.sciencedirect.com

ScienceDirect

Advances in Space Research 77 (2026) 9462–9482

ADVANCES IN SPACE RESEARCH (a COSPAR publication)

www.elsevier.com/locate/asr

A newly identified disturbing effect in the LISA pathfinder test mass release into geodesic

Abraham A. Gelan [a,b,*], Matteo Tomasi [a,b], Edoardo Dalla Ricca [a,b], Francesco Marzari [a,b,c], Carlo Zanoni [a,b,c], Daniele Bortoluzzi [a,b]

[a] *Department of Industrial Engineering, University of Trento, Via Sommarive 9, Trento 38123, Italy*
[b] *National Institute for Nuclear Physics (INFN), Via Sommarive 14, Trento 38123, Italy*
[c] *Department of Physics, University of Trento, Via Sommarive 14, Trento 38123, Italy*

Received 24 September 2025; received in revised form 15 February 2026; accepted 3 March 2026
Available online 6 March 2026

Abstract

In LISA (Laser Interferometer Space Antenna), the first observatory of gravitational waves from space, a Grabbing, Positioning, and Release Mechanism (GPRM) is designed to inject a 1.96kg test mass (TM) into a geodesic trajectory, with residual velocities (with respect to the hosting spacecraft) below 15μm s^{-1}(linear) and 500μrad s^{-1}(angular). During LISA Pathfinder (LPF), a technology demonstrator mission flown by ESA in 2015, several injections exceeded these requirements due to unintended recontacts between the mechanism main end-effector (plunger) and the released TM. This was caused by the erosion of the micrometric gap between the TM and the plungers in the preliminary maneuvers, preparatory to the nominal TM injection to be performed by dedicated end-effectors (release tips). We identify premature TM releases, evidenced by TM displacements and rotations non compatible with the mechanism holding action, taking place before the nominal injection instant, i.e. the separation of the release tips from the TM. At the same time, an interfering fictitious force signal, generated during the release tip extension, can mimic the presence of contact between the tips and the TM, producing conflicting diagnostic signals (i.e. false confirmation of held TM). Ground tests and FEM analyses show that this interference originates from the plunger deformation near the force sensing element. Using the LPF telemetry and a multibody model including the origin of the interference, we reproduce the in-flight LPF release tests signals and trace the root cause of the premature releases. Our results highlight the opportunity to integrate force sensing into the control loop during the TM handover from plungers to release tips, and identify the mechanism stiffness required to suppress the fictitious forces for the LISA GPRM. We also outline improvements to the release procedure to enhance its reliability in the upcoming LISA mission.

Keywords: LISA Pathfinder; Space mechanism; Mechanism dynamical model; Injection into geodesic motion; Mechanism in-flight testing

1. Introduction

Identifying critical anomalies and optimizing design and control strategies are essential for mechanisms used in scientific space missions that require highly accurate system functionality. One such mechanism is the Grabbing, Positioning, and Release Mechanism (GPRM, Bortoluzzi et al. (2009, 2013, 2007)), designed to release a

* Corresponding author.
E-mail addresses: abrahamayele.gelan@unitn.it (A.A. Gelan), matteo.tomasi-1@unitn.it (M. Tomasi), edoardo.dallaricca@unitn.it (E. Dalla Ricca), francesco.marzari-1@unitn.it (F. Marzari), carlo.zanoni@unitn.it (C. Zanoni), daniele.bortoluzzi@unitn.it (D. Bortoluzzi).

https://doi.org/10.1016/j.asr.2026.03.011
0273-1177/

gold-platinum test mass (TM) into a geodesic trajectory, to start the scientific phase of the LISA mission (Laser Interferometer Space Antenna, Amaro-Seoane et al. (2017, 2008)). Scheduled for the mid-2030s (Amaro-Seoane et al. (2017)), LISA is a major European Space Agency project designed to detect gravitational waves in space (Bell (2008)). LISA comprises three spacecrafts positioned at the vertices of an almost equilateral triangle, with a 2.5 million kilometers side. Each spacecraft contains two TMs set in geodesic trajectories, i.e. determined only by the planetary gravitation. A laser link, in correspondence of the triangular constellation side, pairs two TMs contained in different spacecrafts, measuring the relative distance between them. By isolating all other sources of disturbance, the system ensures the gravitational waves detection in the frequency range between 0.1mHz and 100mHz.

In 2015, a demonstrator mission, called LISA Pathfinder (LPF, Wanner (2019)), was launched to assess the technology readiness for the LISA mission (Armano et al., 2018; Armano et al., 2016; McNamara et al., 2008). In LPF, a single spacecraft hosted two sensor heads, known as Gravitational Reference Sensors (GRS, Dolesi et al. (2003)), which will be adopted also for LISA. Each GRS unit is equipped with a TM and its associated electrode housing, as well as a caging and venting mechanisms (CVM, Zahnd et al. (2013)) and a GPRM. The TM is enclosed in an electrode housing, which shields the TM and provides the TM simultaneous actuation and sensing, by using a set of electrodes. The electrodes are biased using a high frequency voltage signal during the sensing operation, providing accurate estimation of TM position and attitude through capacitive measurements at the electrodes. However, the bias signal can interfere with some the GPRM equipment, increasing their read out noise. For this reason, the bias is switched off during the most delicate mechanism operations.

During launch, a high pre-load force is applied by the CVM to the TM eight vertexes, to hold it and to protect the electrode housing from potential impacts caused by the high launch accelerations. When the spacecraft reaches the desired orbit, the eight fingers of the CVM are retracted, transferring the responsibility of holding the TM to the GPRM. The GPRM consists of two nearly symmetrical units. Each GPRM unit is equipped with two end effectors (see Fig. 1)) to hold the TM and release it with a linear momentum of less than 10kg μm s^{-1} and an angular momentum of less than 200kg μrad s^{-1}. The primary pair of end effectors, known as plungers, is used to grab and center the TM. The plungers have a pyramidal or a conical head that engage the TM in two opposed indents on the TM surfaces (see Fig. 2). The plungers are actuated along the Z-axis (see Fig. 1a) by custom PI-Nexline piezo walker actuator. The walkers move a linear runner, which connected to the plunger by a compliant bridge, at the back, and by a flex hinge, at the front. The flexible bridge, at the back of the plunger, is equipped with four strain gauges in full Wheatstone bridge configuration from a constant voltage source to measure the force that the mechanism exerts on the TM interface. A dedicated side-guiding system is used to guide the runner in the plane in which the Nexline is not present (see Fig. 1b). Two small tips, coaxial with the respective plungers, constitute the secondary mechanism's end effectors. The tips are actuated by a stack unit composed of two piezo-stack actuators, one nominal and one redundant. These actuators extrude/retract the tips from the plunger head by deforming a preloaded washer spring. The extruding tips engage the TM indents in two dedicated surfaces, called landing areas (LA).

To meet the strict requirements on the TM linear and angular momentum, a release strategy is adopted in LISA Pathfinder consisting in four main phases: grabbing, force relaxation, handover, and tip retraction (see Fig. 3). During the grabbing phase, the GPRM plungers heads move toward the TM and engage the two indents at the two opposite sides of it. When the contact force measured at the force sensor reaches a threshold value (2N nominal in LPF) the grabbing process is stopped. To perform the release, first, the holding force is relaxed by retracting the plungers (force target value in LPF 0.1÷0.3N). Then the handover is performed at one unit at a time, with a combined extension of the tip and retraction of the plunger.

At the end of the handover, the TM is in pre-release condition, held by the two tips and separated from the plunger heads by a small gap (nominal 10μm for LPF). The TM release is performed with a rapid and synchronous retraction of the tips to break their adhesive bonds with the TM (Bortoluzzi et al. (2011a, 2024)), which remains free floating and is captured by the electrostatic actuation system.

Prior to the LPF mission, analyses on the contributions to TM residual velocity were limited to studies of impulses in nominal release (Bortoluzzi et al. (2010)), i.e. a release without recontact between the plunger and the TM. In such condition, the TM momentum is directed only along the z-axis, produced by the asymmetry of the contact forces between tips and TM on the opposed landing areas (Benedetti et al., 2008; Bortoluzzi et al., 2013). Nominal factors were studied, including impulses induced by adhesion bonds between metallic surfaces(Benedetti et al., 2008), time delay in retraction time of the tips, and different retraction velocity of the two GPRM units (Bortoluzzi et al., 2013; Bortoluzzi et al., 2010), in addition to integration and manufacturing tolerances (Koker et al., 2013). The residual impulses are intensified by the contact preload force, therefore this has to be minimized in the release procedure which will be implemented for LISA.

During LPF operations, the GPRM realized non-nominal TM releases with momentum components out of the z-axis. After commissioning and prior to the end-of-mission campaign, all the TM releases were manually executed by the operator, with the electrostatic actuation enabled only after the TM state vector estimate reached sufficient accuracy and resulted fairly centered and aligned. This strategy was not always successful, sometimes

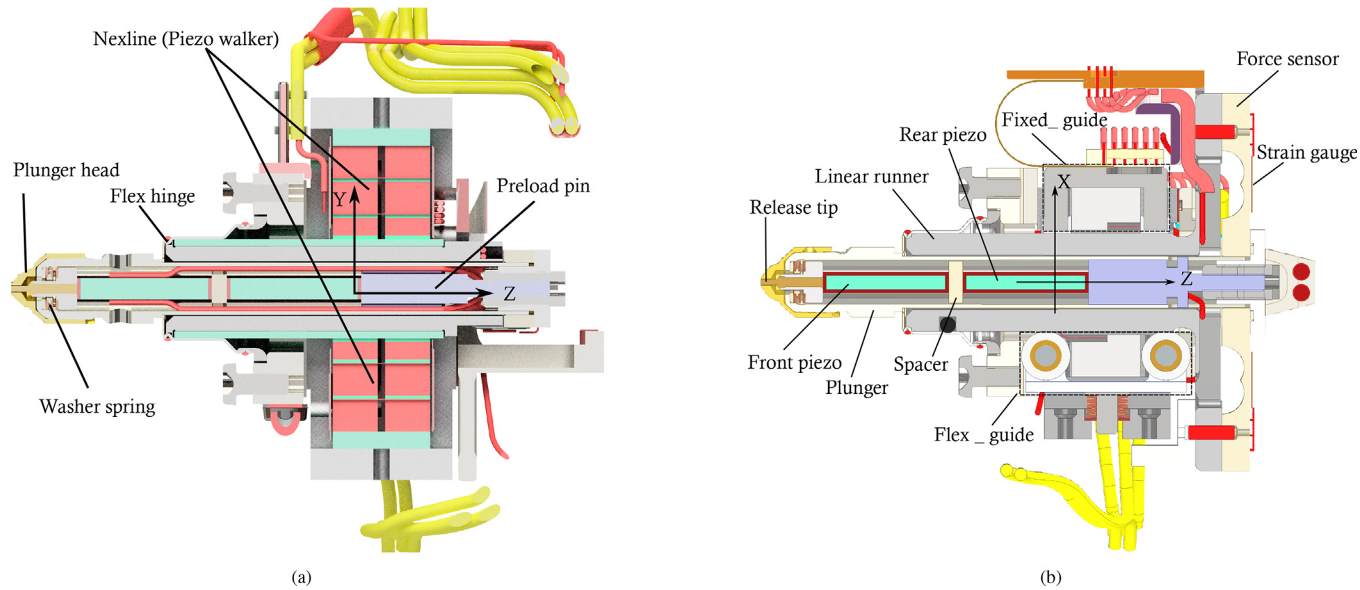

Fig. 1. The figures show a section of the LPF GPRM unit. In A, a y-z sectional view of a GPRM unit is shown, where the linear runner is moved along the z-axis by the Nexline. In B, an x-z sectional view of the same GPRM unit is depicted, where the T-shaped linear runner is constrained by a slider guide and two spring-loaded rollers.

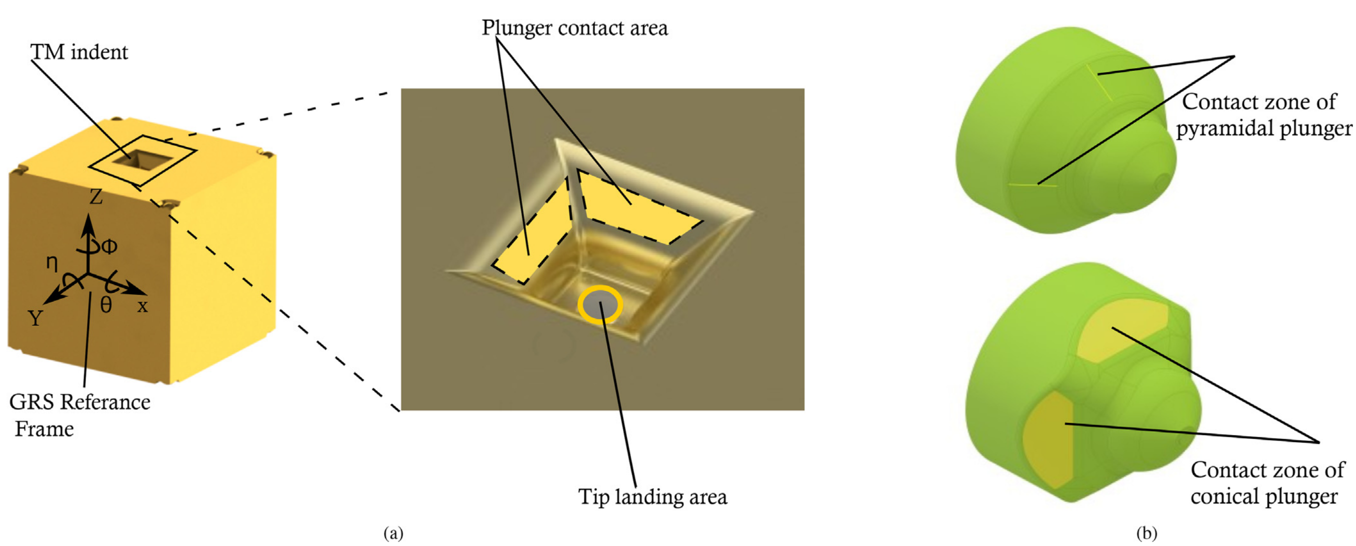

Fig. 2. In A, an image of the cubic TM is depicted. A magnified view shows the indent geometry on the z faces of the TM, where the plunger heads fit. The surfaces acting as interfaces with the plungers and the tip are highlighted. In B, the geometry of the plunger heads is shown: conical (Z^- side of the TM) and pyramidal (Z^+ side of the TM) - Credits: (Bortoluzzi et al., 2021b).

requiring TM re-grabbing and releasing again, and was feasible thanks to the short two-way light travel time,which is 10 s, enabling timely ground intervention (Bortoluzzi et al., 2021b).

In LISA the much longer two-way light travel time of approximately 6 min precludes ground-assisted control and therefore requires automated release procedures. The current LISA baseline does not include the automation of the LPF trial-and-error approach, which produced impacts and TM bounces on the plungers, requiring repeated attempts (Bortoluzzi et al., 2021b). Part of the extended mission was dedicated to investigate this anomalous GPRM behavior (Bortoluzzi et al., 2021a). The releases were characterized by excessive velocities resulting from recontact between the plunger and the TM during the tips' and plungers' retraction, attributable to the erosion of the micrometric gap between the plunger head and the TM indent (Bortoluzzi et al., 2021a; Tomasi et al., 2023; Dalla Ricca et al., 2025). Post-LPF investigations focused on achieving nominal TM releases by addressing gap erosion problem. Factors including mechanism vibrations during release tip retraction (Bortoluzzi et al., 2021a; Vignotto, 2021), misalignment between two GPRM units (Tomasi et al., 2023; Vignotto, 2021), and anomalous

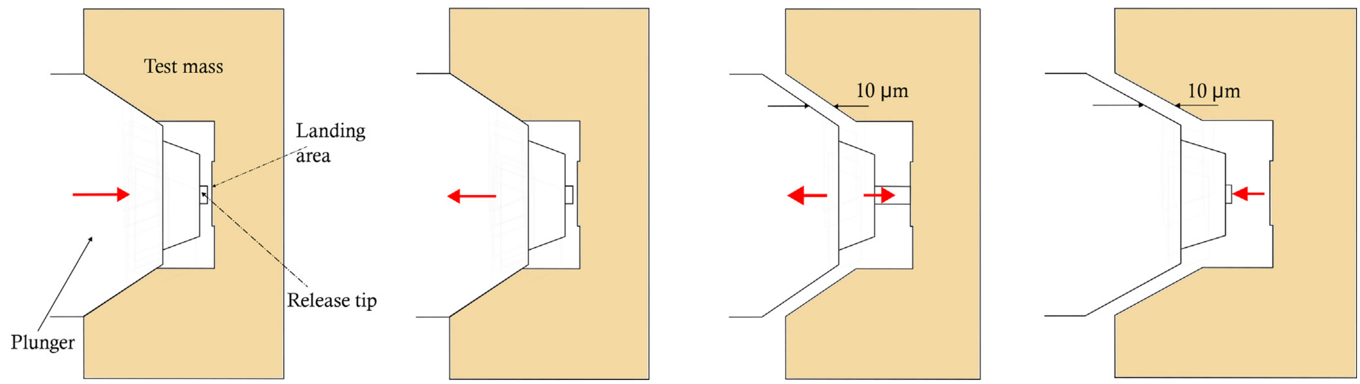

Fig. 3. The scheme describes the nominal TM release procedure adopted for LPF TM release. The first figure illustrates the *grabbing process*, with the red arrow indicating the direction of the plunger's motion during the grabbing stage. The second figure shows the *force relaxation*, where the plunger is retracted a bit to decrease the preload on the TM. In the third figure, the *handover process* is illustrated, with the red arrows depicting the coordinated motion of the tip and the plunger. Finally, the fourth figure shows the *tip retraction*, which corresponds to the nominal release instant. On the opposite TM side the same steps are performed.

plunger trajectories (Vignotto et al., 2023) are investigated. These effort prompted delta design of the LISA GPRM, such as improved side guiding system and increased release tip stroke (Zanoni et al., 2024).

The TM dynamics after a nominal release is that of a free-floating body, either subjected mainly to the spacecraft self-gravity (first 10 s before switching on the control loops) or controlled through the electrostatic actuation. The open-loop dynamics of the TM has a confined time-frame (about 10 s) and may be affected by negligible non-nonlinearities (influencing the trajectory of about 1 part over 1000). The closed loop dynamics is ruled by a sliding-mode controller (Montemurro et al., 2006), specifically designed to handle nonlinearities, noise, actuator saturation, and modelling uncertainties, driving the TM state to equilibrium. Its robustness was validated through Monte Carlo simulations and confirmed during flight (Schleicher et al., 2018), where releases exhibiting larger-than-expected velocities and overshoots were still successfully captured and stabilized. In both open and closed loop state after release, the TM dynamics results largely predictable, being the non-linearities negligible (open loop) or subjected to a closed-loop control system.

Starting from the flight heritage of the LPF GPRM, an alternative release mechanism is under development at the University of Florida, for a Simplified Gravity Reference Sensor (SGRS), aiming at future earth geodetic missions (Dávila Álvarez et al., 2022; Conklin et al., 2025). The concept of this launch-lock and release mechanism is similar to the LPF design. Since the proof mass is lighter (about 1/4), the caging function is performed by the plungers (no CVM) and the release function is performed by two passive tips actuated by springs (instead of piezo stack actuators) to enhance simplicity (Footdale et al., 2024).

Another notable mechanism is the release system developed for the Mobile Asteroid Scout (MASCOT), a nanoscale surface package designed for the exploration of small Solar System bodies (Grimm et al., 2019). The mechanism deploys the landing module (LM) in a microgravity environment (Grimm et al., 2020). Its primary objective is to release the LM while ensuring it remains on the surface after deployment, preventing rebound into space. The mission was successful, even though the allowable release velocity was significantly less stringent than that required for the LISA mission.

In this work, we address a newly observed anomaly in the in-flight release of the TM. The handover procedure, preceding the release, is identified as critical since it relies on a limited gap margin to avoid unwanted contacts. Specifically, we observed that some anomalous releases are produced by a premature separation between the TM and the holding tip/plunger at the handover phase, obscured by an unexpected interference of the tip extraction with the contact force signal. The premature TM floating state is detected through its position and attitude telemetry signals, which show significant variation before the retraction of the tips. This premature TM motion brings to uncontrolled re-contact with the plungers and momentum transfer at the retraction of the tips and the plungers.

One possible origin of the missing detection of the premature floating state is investigated by testing the qualification model of the LISA Pathfinder GPRM, where a fictitious force signal is observed during the free extension of the release tip, without any body contacting either the plunger or the tip. Further ground tests and FEM analyses indicate that the cause of the fictitious force signal is the deformation of the plunger produced by the free extension of the release tip.

Given the criticality of the handover procedure for the release, we develop a multi-body model that embodies this anomalous behavior, and analyze the performance of the handover by simulating the LPF release procedure. In our analysis, we consider a free TM and two independently actuated GPRM units, representing the in-flight configuration. The nominal release procedure, resembling the one used in LPF, is implemented in MATLAB Simulink, and a co-simulation technique is employed using MSC Adams for the overall system dynamics. This approach allows us to study in detail the handover and release phases, addressing the mechanism compliance, load paths through the mechanism components (flex hinge, force sensor, plunger), force sensor sensitivity to local distortion, and fictitious force signal, while simultaneously examining the effective contact interactions between the TM, the plunger and the release tip.

Simulations of the LPF release procedure revealed key factors contributing to premature release and potential issues of workaround strategies, including the force sensor responses in the presence of plunger deformation. Leveraging the developed GPRM model, a requirement on the stiffness of mechanism's components is set to reduce the fictitious forces observed on ground. It's believed that reduction of fictitious force will provide a more reliable diagnostic signal for improving the TM injection procedure. Additionally, we also analyzed other stages of the LPF release procedure and proposed complementary risk-mitigation strategies.

The subsequent sections are organized as follows. Section 2, focuses on the analysis of in-flight data, addressing the unexpected TM floating state during prerelease. In Section 3, the role of release procedures in the observed floating condition is investigated. The correlation with the plunger penetration in the TM indents and the handover operation is explained. In Section 4, we present the ground testing of the GPRM and validate a hypothesis regarding the origin of the fictitious force observed in the mechanism. We also show the extended analysis of fictitious forces for the flight model (FM) of the GPRM. In Section 5, we present the construction of the multibody model, which is based on a validated lumped parameter model of the GPRM, and includes detailed models of the piezo actuator, the Nexline actuator, and the implemented control system used in the analysis. Section 6 presents the results and discussion of the analysis, highlighting key findings. Finally, Section 7 concludes the paper, summarizing the main outcomes and outlining potential directions for future work.

2. In-flight tests in the LPF extended mission and premature TM releases

Due to the anomalies occurred in the initial LPF GPRM TM releases (Bortoluzzi et al., 2021a), several tests with various injection procedures were performed at the end of the mission to identify their causes and possible mitigation strategies. A total of 110 TM release tests were conducted for each TM contained in the two LPF GRSs (TM1 and TM2).

The telemetry of the release tests includes the linear and angular position of the TM, the position of the Z^+ and Z^- linear runner, the position of the tips, estimated using the piezo-stacks commanding voltage, and a boolean signal associated to the plunger bias state (on or off), affecting the GPRM force sensor noise. As explained in the introduction, the bias voltage is switched off before the beginning of the handover (in the post grabbed phase) and switched on again during pre-release. The data related to the TM states are available just in specific phases of the GPRM operation, i.e. when the bias is on.

The following analysis focuses just on nominal tests. During the extended phase of the mission, variations of the nominal release procedure have been tested (44 tests in total). Additionally, for some of the nominal releases, the bias signal is switched on just before the tip retraction. This makes that just few sampling points are available in the pre-release phase, making the identification of the system behavior non reliable. In the end, by dealing only with nominal and reliable tests, the following will analyze 42 tests, for TM1 release, and 51, TM2 releases.

Among the phases of the release procedure, the pre-release phase is identified as the period in which the TM is ideally held by the two release tips, with the plungers no longer in contact with the TM. During this stage, the tips are expected to firmly hold the TM until the actual release is triggered by the tips retraction. However, analysis of telemetry data of the TM degrees of freedom sometimes indicates a measurable displacement during this period. This phenomenon is illustrated in Fig. 4, which presents data from a specific in-flight test, showing pre-release TM's position and orientations. This observation suggests that the TM is no longer constrained by the GPRM units, making it plausible that it is already in a free-floating state. This observation motivated a systematic analysis of the potential floating condition across all in-flight tests, by computing the maximum variation of the TM position and orientation signals during pre-release (hereinafter called *delta displacements*).

The preload forces during the pre-release phase are also analyzed for possible correlation with the free-floating condition.

The computation of the preload force of the tests is performed by looking at the force difference, measured by the force sensor, before and after the tip retraction. Fig. 5 reports a demonstrative example of force signal in correspondence of the tip retraction instant. ΔF is the force difference between the measured force value before and after the retraction, F_{pre} and F_{post} respectively, computed as the average of the green parts of the curve in Fig. 5.

σ_{pre} and σ_{post} are the standard deviations of the values of F_{pre} and F_{post}. The computation of ΔF, and its standard deviation, is performed according Eq. 1, where $i = [Z^+, Z^-]$ since it is computed independently for the two GPRM units.

$$\Delta F_i = F_{\text{pre},i} - F_{\text{post},i}, \\ \sigma_{\Delta F_i} = \sqrt{\sigma^2_{\text{pre},i} + \sigma^2_{\text{post},i}} \tag{1}$$

Then, the two preloads, estimated at the two sides of the TM, are combined statistically by using Bayesian theorem

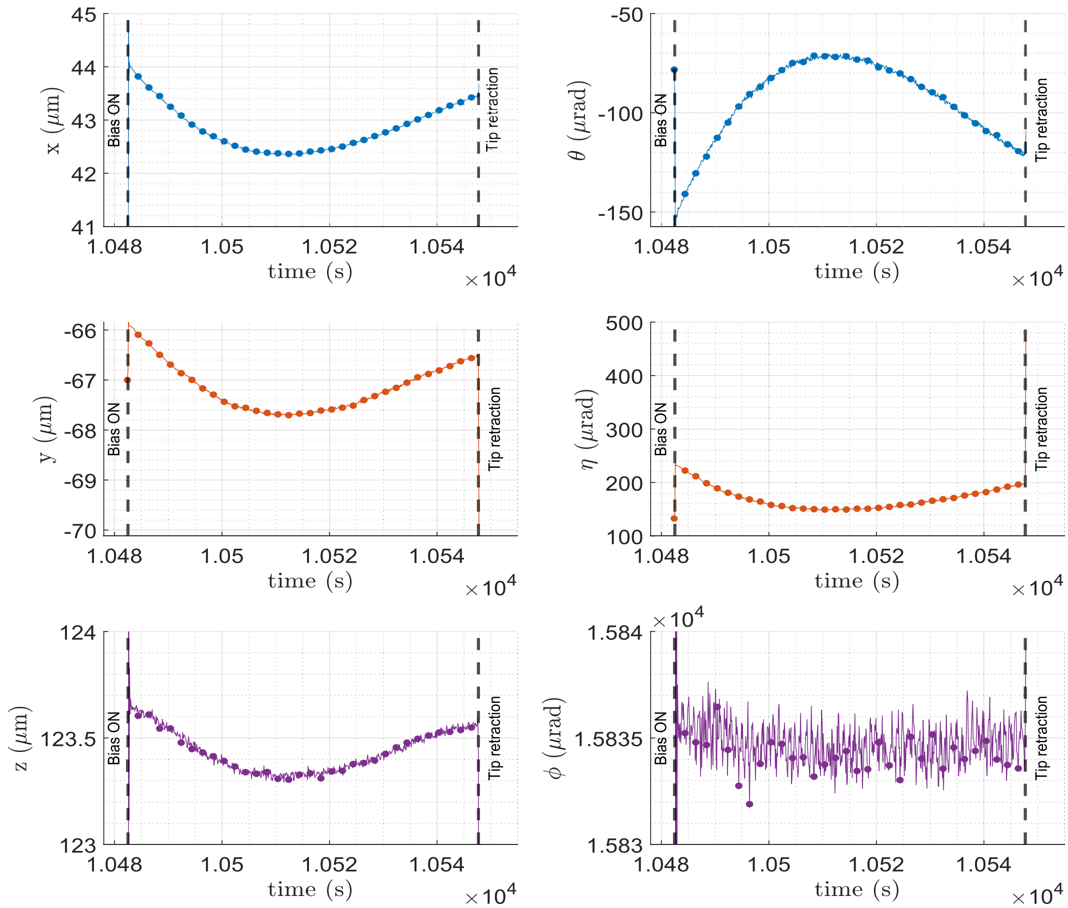

Fig. 4. The figure illustrates the in-flight TM pre-release displacement measured during a test in the extended mission of LPF on 29 June 2017, Test ID [0401](TM1). The measurements reveal significant motion of the TM across all degrees of freedom. Black dashed lines mark the instant when the bias is switched on and the tip retraction instant. The preload force applied to the test mass (F) is 0.04 ± 0.07N.

(Vignotto (2021), see Eq. 2) to find the preload value F, with its uncertainty σ_F.

$$F = \frac{\sigma^2_{\Delta F_{Z-}} \Delta F_{Z+} + \sigma^2_{\Delta F_{Z+}} \Delta F_{Z-}}{\sigma^2_{\Delta F_{Z-}} + \sigma^2_{\Delta F_{Z+}}}, \qquad \sigma_F = \sqrt{\frac{\sigma^2_{\Delta F_{Z+}} \sigma^2_{\Delta F_{Z-}}}{\sigma^2_{\Delta F_{Z+}} + \sigma^2_{\Delta F_{Z-}}}} \tag{2}$$

2.1. Test Mass Motion During Preliminary Operations

In Fig. 6, we show pre-release delta displacements vs preload forces for all the in-flight tests performed for the TM1 and TM2 during the extended mission. In the figure, it is expected that the TM shows a significant delta displacement only when the preload force is compatible with zero, i.e. no contact is present between TM and tips. However, in some tests a delta displacement is detected even with a preload force in the range of 0÷0.1N. This inconsistency highlights a potential interference on the force sensor signal present during the mechanism operation, and its limited meaningfulness in the detection of TM-tip contact. This will be addressed in Section 4 as the *fictitious force* signal issue.

3. The role of Release Procedures in the observed premature releases

As mentioned in the introduction, the nominal release procedure consists of four steps: grabbing, force relaxation, handover, and TM release. Among these, the grabbing and TM handover phases are particularly delicate as they can potentially lead to premature release. Inaccurate grabbing, for instance, can result in insufficient penetration of the plunger into the TM indent, causing a misalignment of the TM that propagates to the subsequent steps, especially during handover. The handover itself is inherently critical since non perfectly coordinated plunger retraction and tip extension can also trigger an unintended release. To address these, the following two sections are dedicated to a detailed analysis of these procedures. First, we investigate the penetration of the plunger into its indent relying on telemetry data. Then, we provide a brief discussion of the

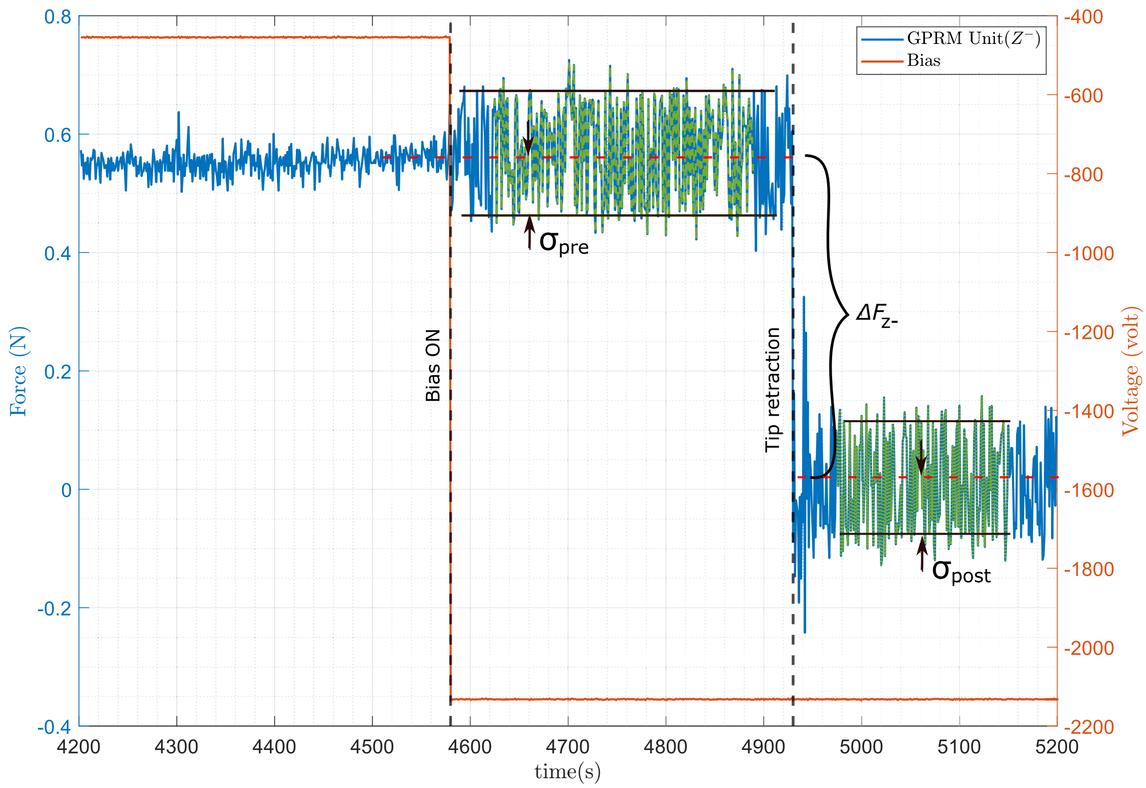

Fig. 5. Force signal during the pre-release phase for the release test performed with TM1 on 29 June 2017 in the LPF mission. ΔF_{z-} represents the difference between the mean of the force (indicated by the red dashed lines) before and after the tip retraction. The force sensor noise increases when the bias is switched on across the release event. The standard deviation of the force signal is represented by the black lines.

handover as implemented in LPF, highlighting specific aspects pivotal for the success of the release procedure.

3.1. The role of the TM grabbing procedure

We investigate and provide insights into how the TM grabbing procedure affects the overall injection phase. We focus on how the plungers penetration in the indents affects the TM position and orientation during the grabbing process and pre-release conditions, relying on the LPF in-flight tests. The co-penetration is defined as the sum of the Z^- and Z^+ GPRMs linear runners positions, quantifying the overall penetration of the plungers in the respective indents. The computation is carried out during two distinct idle phases of the release procedure. The first phase occurs post-grabbing. The second phase is the pre-release state, when the handover at both sides of the TM are already performed. Large values of the co-penetration indicate an optimal fit, associated with a good grabbing process. Subsequently, to have a suitable reference, we subtract the maximum co-penetration value to all the tests, assuming it close to the best fit case. This approach brings the maximum co-penetration to zero, while the lower co-penetration values appear negative (see Fig. 7). If the delta displacement computed during the pre-release phase exceeds the $\pm 3\sigma$ interval (with σ computed in post-grabbing, with a still TM), the TM is considered to exhibit delta displacement. Otherwise, it is categorized as having no delta displacement.

The TM angle around z (ϕ) and the co-penetration during the grabbing phase are correlated by the geometry of the TM indent and the plunger head. The plunger heads are designed with a conical and pyramidal front end (see Fig. 2b), which are intended to fit the pyramidal indentations on the TM surface (see Fig. 2a). During the grabbing process, the plunger and the TM get in contact at the peripheral of the pyramidal TM indent. As the plunger advances by co-penetrating the indent, the contact points on the plunger's head ideally slide along the indent surfaces. Since the TM is initially free, the force applied by the plungers induces a settlement of the TM in all the degrees of freedom. This settlement shall continue until the TM aligns with the plungers, producing optimal engagement between the plunger head and the respective indent. In this configuration, the value of the TM position and attitude inside the housing shall be approximately equal to zero, corresponding to a perfect centering of the TM produced by the maximum co-penetration. However, by analyzing the LPF telemetry data, we observed a significant deviation from this behavior. In particular, it is found that the ϕ rotation, which should be set by the alignment of the pyramidal TM indent with the pyramidal head of the z^- GPRM unit, has a significant dispersion, and the co-penetration is not always maximum. In Fig. 7, we report the plungers co-penetration as a function of the TM ϕ rota-

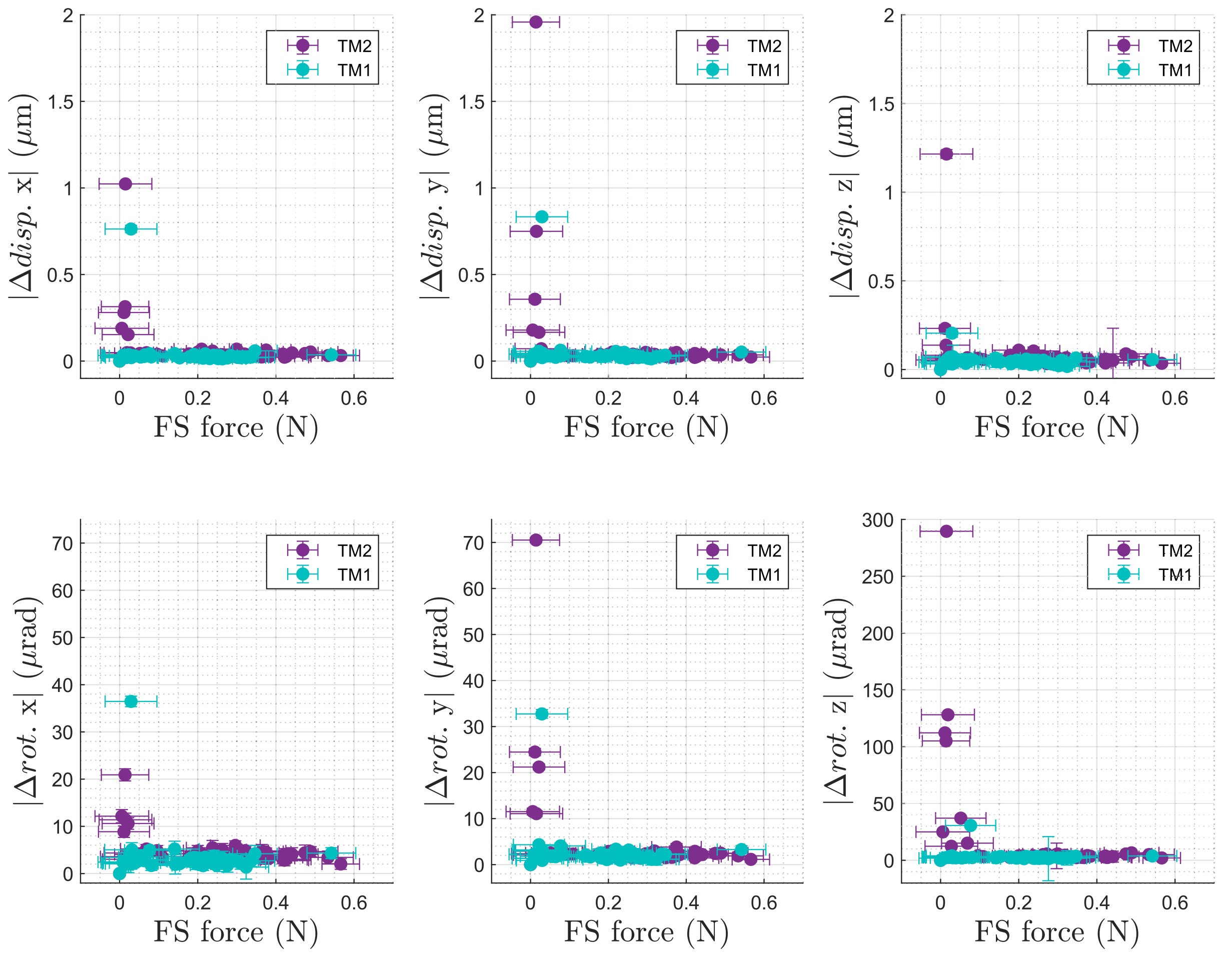

Fig. 6. The figure shows the absolute delta displacement versus preload force of TM1 and TM2 during the pre-release phase, based on 42 tests for TM1 and 51 tests for TM2, conducted during the extended mission of LPF. At lower preload forces, the figure indicates that the TM was already in motion or floating. This occurs across all the degrees of freedom when the TM should remain stationary and be held by the release tips.

tion. In the figure, we can notice that the maximum co-penetration is achieved near 0 ϕ angle, but many TM configurations largely deviate from it.

When the TM misalignment with respect to the plunger in post-grabbing configuration is dominated by the ϕ rotation, the points describing the TM configuration in Fig. 7 result located close to the boundaries (two black-dashed lines), describing the maximum ϕ rotation allowed by the pyramidal plunger with such co-penetration. The points located between the bounds refer to a grabbed TM states with a misaligned configuration not only in ϕ but also in the other degrees of freedoms.

For what concerns the points in pre-release configuration, the handover is already performed, producing plungers retraction and a relative reduction of the co-penetration value. In Fig. 7, we discriminate 3 different conditions observed in the pre-release phase.

1. The case in which no displacement is observed in any of the TM degrees of freedom. This means that the constraint given by the tips is able to hold the the TM.
2. The case in which no displacement is observed in any of the TM degrees of freedom except for the rotation around z (ϕ angle). In this case, the tips may still be in contact with the landing areas but the holding authority of the two tips is not able to constrain the ϕ TM rotation.
3. The case in which a displacement is observed in at least one TM degrees of freedom different from ϕ. This is the evidence that the TM is in floating condition and the tips are not in contact with it.

It is evident that low values of co-penetration are related to misaligned grabbed configurations. This means that the TM do not settle properly on the two plungers, which get stack misaligned inside the relative intent Tomasi et al. (2022). When the TM is grabbed with a limited co-penetration, during the handover the extension of the tip is not sufficient to produce the contact with the TM, due to the large initial distance between the tip and its landing area. Hence, the TM is prematurely released by the retraction of the plunger, justifying the observed large values of the TM delta displacement. This suggest as the TM states

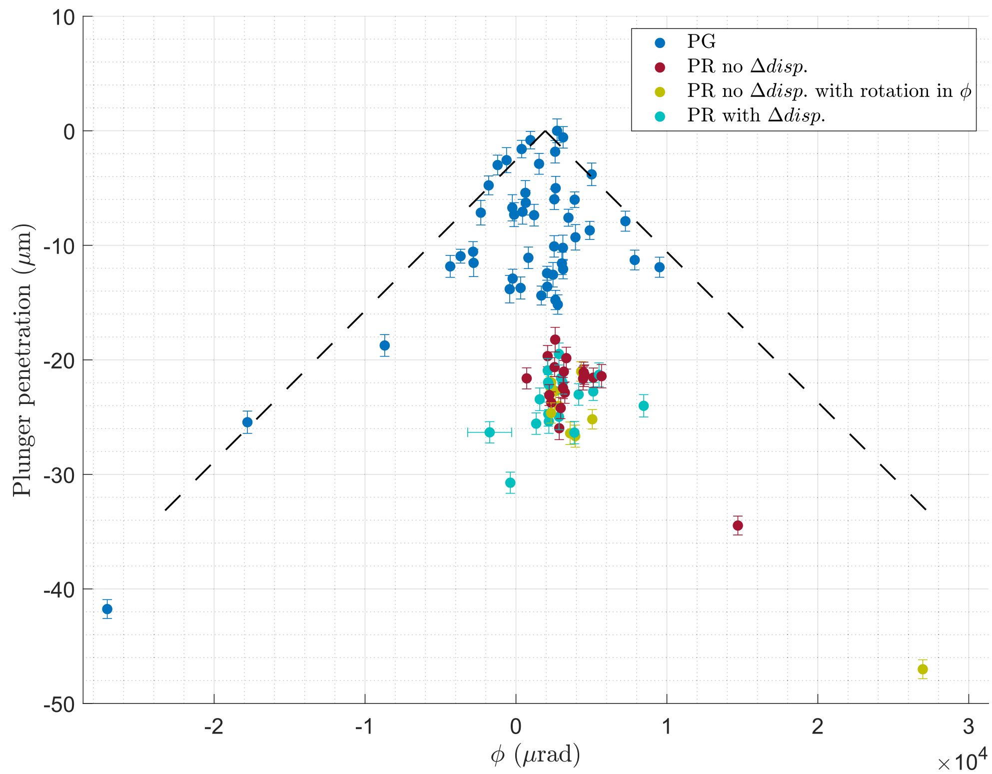

Fig. 7. The figure shows the co-penetration of the plungers into the TM2 indents as a function of the TM rotation around z (ϕ) during the post-grabbing and pre-release phases, based on 51 tests from the extended mission of LPF. The standard deviation for both co-penetration and TM rotation is displayed by error bands.

at the grabbing can give relevant information about the quality of the grabbing process, leading to safer handover.

3.2. The role of TM Handover procedure

The handover of the TM represents a critical phase in the release process of LPF, yet it is not sufficiently examined, particularly in relation to the anomalies observed during flight.

Fig. 8 illustrates the GPRM telemetry signals at the handover, for one of the LPF tests. The handover for the two units, Z^+ and Z^-, is executed independently, occurring at different time intervals. Fig. 8a presents the handover performed at the Z^- unit, while Fig. 8b shows the handover at the Z^+ unit. Although the overall process remains consistent, the two handovers exhibit notable differences in their initial phases.

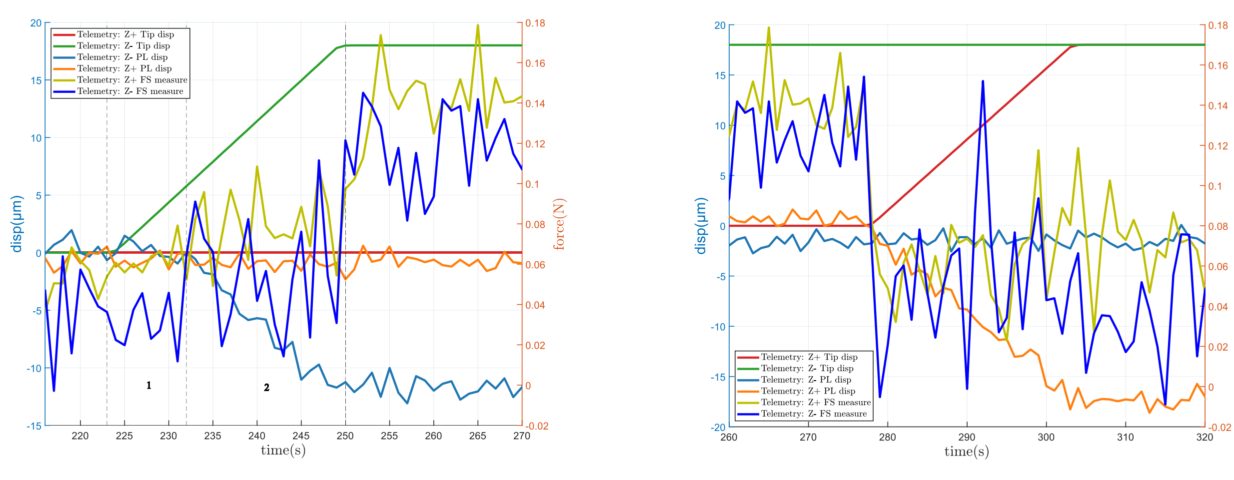

Fig. 8. The figures show the nominal handover performed in LPF on 29 June 2017, Test ID [0302] (TM1). Figure (a) reports the handover in the Z^- unit, while Figure (b) shows the handover at Z^+. The preload forces measured by the force sensor (FS), as well as the displacements of the plungers (PL) and the release tips, are shown.

As can be observed in the initial phase of the first handover (Fig. 8a), the piezo actuator is commanded to extend the release tip while the plunger is stationary. Given that the tip has a free stroke distance (nominal 4μm for LPF) to travel before getting in contact with the LA, the force measured by the sensor remains unchanged until the free stroke is covered and the contact is established. This contact results in a sudden spike in the measured force. The retraction of the plunger starts at the force spike, with a coordinated motion: the release tip extends further, while the plunger retracts. The motion of the release tip and plunger proceed at the same speed until the tip is fully extended (stroke of 18μm). Confirmation of the final tip-TM contact is provided by a nonzero measured force.

Unlike the Z^- case, the Z^+ handover starts without letting the tip reach the landing area (Fig. 8b). The plunger retracts from the beginning, while contact between the release tip and the TM is not set, causing a sharp drop in the force measured by both sensors. In this condition, the TM is released by the plungers and moves uncontrolled in the narrow gap created by the plunger retraction, not being compensated by the tip extension. After this handover, a false confirmation of tip-TM contact is provided by the measured force (about 0.05N in Fig. 8b).

4. Fictitious Contact Force Signal in the Qualification and Flight Models of the LISA Pathfinder GPRM

During the LPF GPRM EQM testing activities, a force with a magnitude of 0.11N was measured on the Z^- unit when the tip was completely extended, extruding of approximately 16μm from the plunger head, with no external preload applied to the mechanism. This fictitious force reading is clearly an interference on the force signal, generated by the tip extension.

Fig. 9 shows the force measured by the EQM force sensor during a free-extension of the tip. The force interference can hinder the interpretation of the handover during in-flight release by masking the absence of a real contact with a fictitious force generated by the tip extension. To address this issue, we investigate the origin of the force interference with ground testing. Furthermore, since the qualifying model and the flight model present small differences, we extend our analysis of fictitious forces to the flight model, relying on telemetry data from the mechanisms to characterize their effects.

4.1. On-ground testing of the GPRM qualification model

To investigate the interference issue, a dedicated test setup was used in the Space Applications Laboratory at the University of Trento (see Fig. 10). The test setup includes two QMs of the LPF GPRM units (Z^+ and Z^-), two laser interferometers and an anti-vibration platform.

Two separate test setups were employed to measure the steady state free distortion of the back side and the head of the plunger at the extension and retraction of the tip. In the first test an interferometer is pointed to the rear end of the plunger (configurations indicated as *Z Back* in Fig. 11). In the second test, a laser interferometer is used to measure the axial motion of the plunger head. Given the shape of the head, the laser is pointed to a small removable mirror (see Fig. 11b), specifically designed for this test. Since the mirror weight acts orthogonally with respect to the plunger axis, it is not expected to modify the steady state distortion.

Fig. 12a shows the motion of the back side of the plunger in response to the impulsive tip retraction, and Fig. 12b displays the motion of the head during the slow extension and fast retraction of the tip. In both cases, no external forces are applied to the mechanisms. We observe a system-

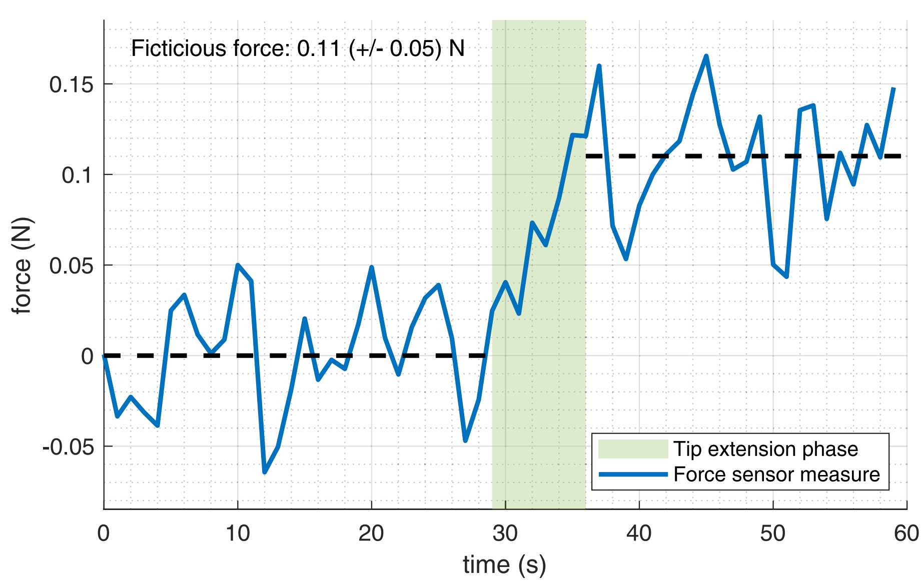

Fig. 9. Force measured during a free extension of the tip, i.e. without any external action acting on the mechanism, for the Z^- EQM unit. The phase in which the tip extends is highlighted. Black dashed lines marks the average force value before and after the tip extension.

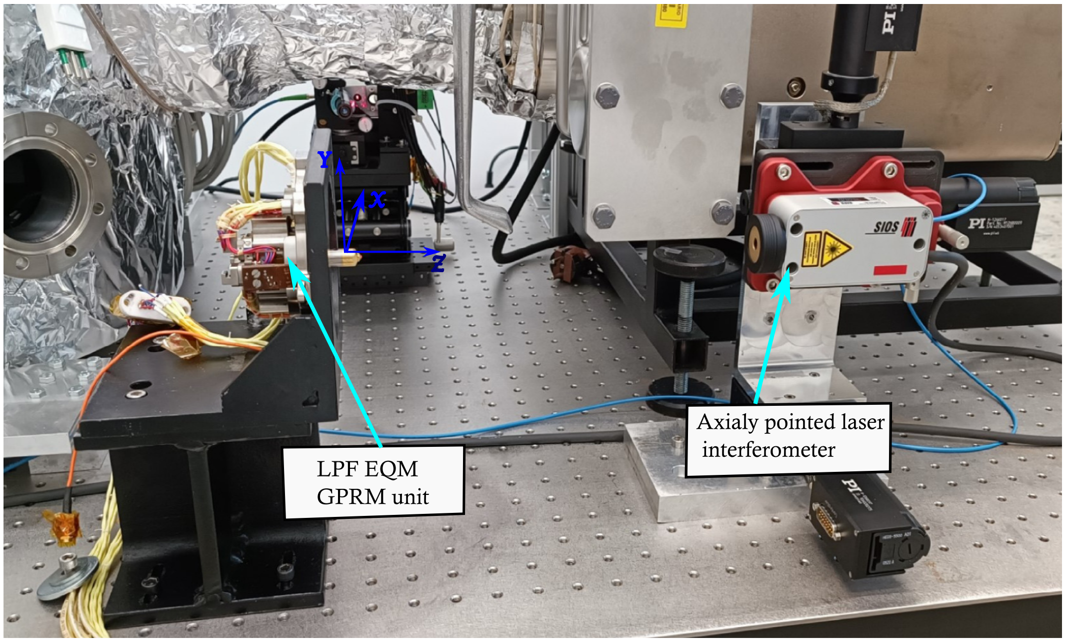

Fig. 10. Ground test setup at the University of Trento for measuring the motion in the front and rear displacement of the GPRM. The setup includes a EQM version of the LPF GPRM units and a laser interferometer. Everything is installed on an anti-vibration platform.

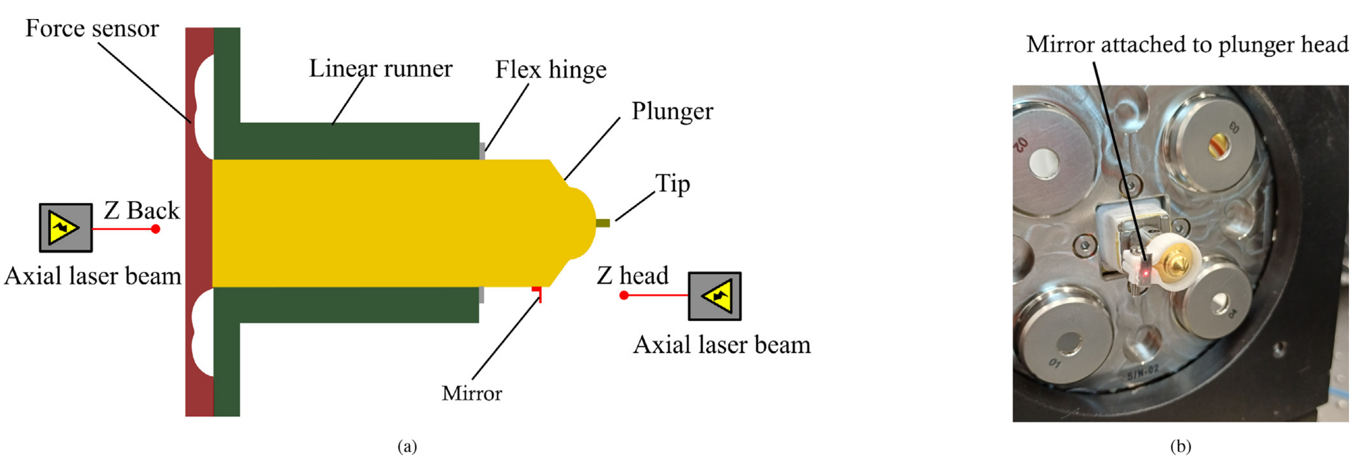

Fig. 11. (a) presents a schematic highlighting the key locations where the laser is directed for measurement, along with other critical parts of the mechanism. (b) displays the mirror mounted on the head of the plunger.

atic offset between the plunger back side position with the extended tip (initial signal at about -0.06μm) and the steady state position after the tip retraction (zero).

During the free tip extension, we observe a linear trend in the position of the plunger head until the tip stops (see Fig. 12b from 7 to 15 s). The tip remains extended until approximately 26÷30s and, when it is retracted, the plunger head returns to its original position.

The axial distortion of the plunger is estimated as the difference between the configuration with the fully extended tip, and the one with the retracted tip. The motion of the two plunger sides, in opposite directions, is compatible with an elastic deformation of the hollow plunger under the effect of the extension of piezo-stack actuator. Simplifying the system dynamics, we assume that the axial compliance of the plunger is modeled by a simple spring, with stiffness K_{PL}, localized in between the two plunger constraints: flex hinge, at the front, and force sensor hinge, at the back.

The two models reported in Fig. 13 represent two possible ways for modeling the GPRM axial dynamics. The stack unit is made by the two piezo-stack actuators, represented by the two springs K_{PZ}, the release tip (TP), and a spacer (SP). The disk spring preloading the stack unit is represented with K_{DS}. The model in Fig. 13a has a non deformable plunger (PL) and the internal force generated by the extension of the piezo (F_{PZ}) does not produce any deformation, except for the tip extension. On the contrary the model in Fig. 13b considers a deformable plunger, with compliance localized in K_{PL}. The action coming from F_{PZ}

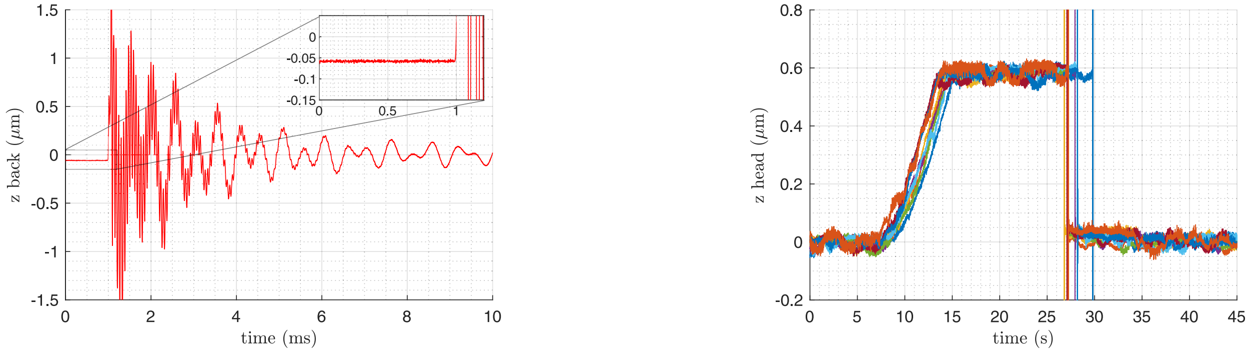

(a) (b)

Fig. 12. (a) illustrates the distortion of the plunger back wile the tip is retracted. (b) depicts the distortion of the plunger head produced by the tip actuation. Both refers to the Z^{-} unit. In the measurement of the plunger back motion (left) the ensemble mean of 10 tests results significantly larger than the ensemble standard deviation, which is not depicted. A focus is given on the initial distortion produced by the tip extension. In the measurement of plunger head (in the right), we can recognize 5 phases: a first steady part, in which the tip is still; a ramp phase, in which the tip if freely extended; a second steady phase, with the extended tip; a quick phase characterized by spikes generated by the tip retraction; and a final steady phase with the retracted tip.

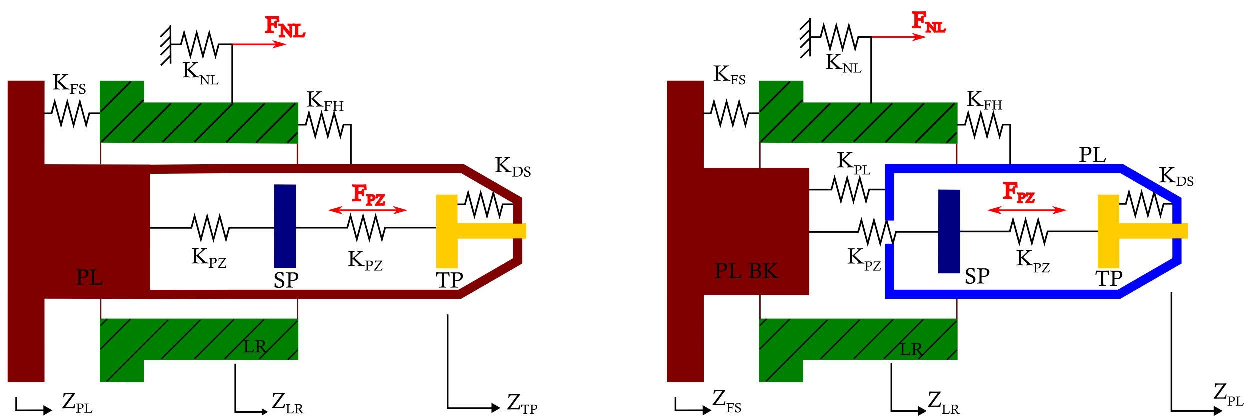

(a) (b)

Fig. 13. In (a), a model of the GPRM axial dynamics is shown. In this model, the plunger is non-deformable under the effects of the internal force F_{PZ}. In (b), an alternative model is reported, considering the axial plunger compliance (localized in the parameter K_{PL}).

produces a stretch of K_{PL}, reflecting in a proportional deformation of K_{FS} and K_{FH}.

The plunger displacement at the back deforms K_{FS} and is converted into a fictitious force measurement by the strain-gauges installed on the force sensor hinge for reading the GPRM preload on the TM during operation. Indeed, the value for the fictitious force can be computed by Eq. 3, in which we can consider Z_{LR} as equal to zero, since the linear runner does not move during a free extension of the tip.

$$F_{FS,\text{freetip}} = F_{\text{fictitious}} = K_{FS}\,(z_{LR} - z_{FS}) = -K_{FS}\,z_{FS} \tag{3}$$

Table 1 summarizes the estimated axial (plunger head and plunger back) steady state distortion of the GPRM plunger, estimated by the ground test results. By using the expression in Eq. 3, with the inputs from Table 1, we can compute the stiffness of the force sensor: $K_{FS} = (1.89 \pm 0.3) \times 10^{6}$ N m^{-1}, for the Z^{-} unit (Z^{+} force signal is not available). The result of this computation is compatible with the outcome of a finite element analysis on the force sensor component, which returns $(1.92 \pm 0.09) \times 10^{6}$ N m^{-1}.

4.2. Fictitious Force Analysis in the LISA Pathfinder GPRM

Ground testing of the LPF EQM revealed the cause of the fictitious force. However, the materials and the integration process of the GPRM flight model were slightly modified, making the EQM not fully representative of the flight hardware. Therefore, it is essential to identify the presence of the fictitious force in the flight hardware, and evaluate its relation with the premature free-floating conditions observed in LPF, discussed in Section 2. On this end, we conduct an analysis based on data acquired during in-flight tests. For selected tests, three specific idle time intervals are selected for such evaluation. During the idle time, both the units are still producing no variation in the force value. This allows to compute the average value of the

Table 1
Steady-state distortions for GPRM Z^+ and Z^- units. The uncertainty is in the order of 5×10^{-3}μm.

Measure	Z^+ unit	Z^+ unit	Units
Z back	-6.9×10^{-2}	-5.8×10^{-2}	μm
Z head	5.81×10^{-2}	5.82×10^{-2}	

measured force, respectively F_{Z^-} and F_{Z^+}, for the Z^- and Z^+ unit, with their standard deviation. For this reason, the selected tests present sufficiently long idle phases to average the force signal and obtain reliable force values (see Fig. 14). The selected idle periods are:

- before Z^- handover (BH1), defined as the idle period following force relaxation;
- after Z^- handover (AH1), which is the idle period immediately following the Z^- handover, corresponding to the period before the handover at the Z^+ unit;
- after Z^+ handover (AH2), the idle period following the Z^+ handover.

During these phases, the measured force signal comprises several components: the true preload force (respectively F_0, F_1, F_2), the stochastic noise contributions from various sources (F_{n_1}, F_{n_2} at the Z^- and Z^+ unit respectively), the force sensor bias (b_1, b_2 at the Z^- and Z^+ unit respectively), and a presumed fictitious force (F_{f_1} and F_{f_2} at the Z^- and Z^+ unit respectively), supposed to arise in each unit after the full extension of the corresponding tip.

Considering this, we can write:

$$\text{BH1}: \quad \begin{cases} F_{Z^-} = F_0 + F_{n_1} + b_1 \\ F_{Z^+} = F_0 + F_{n_2} + b_2 \end{cases} \tag{4}$$

$$\text{AH1}: \quad \begin{cases} F_{Z^-} = F_1 + F_{n_1} + F_{f_1} + b_1 \\ F_{Z^+} = F_1 + F_{n_2} + b_2 \end{cases} \tag{5}$$

$$\text{AH2}: \quad \begin{cases} F_{Z^-} = F_2 + F_{n_1} + F_{f_1} + b_1 \\ F_{Z^+} = F_2 + F_{n_2} + F_{f_2} + b_2 \end{cases} \tag{6}$$

In Eqns. (4)–(6) the distinction between force noise and bias is based on the timescale of observation of the signals (tens of seconds). Any bias contribution accounts for noise frequency components much smaller than the inverse of the observation time and can be assumed as a constant in the observation time. Conversely, any noise contribution accounts for noise frequency components larger than the inverse of the observation time, can be seen as a zero-mean random variable and its effect can be reduced by averaging the signal. In Eq. 5 and Eq. 6, the presence of a fictitious force becomes evident in the scenarios involving handover operations. Specifically, Eq. 5 introduces the fictitious force (F_{f_1}) contribution in the GPRM Z^- during the first handover, while Eq. 6 incorporates both the fictitious components F_{f_1} and F_{f_2}.

Given the symmetric design of the GPRM, it is possible to eliminate the contribution of the preload by computing the difference between the mean force measured at Z^+ and at Z^-, for each phase. This approach isolates the differen-

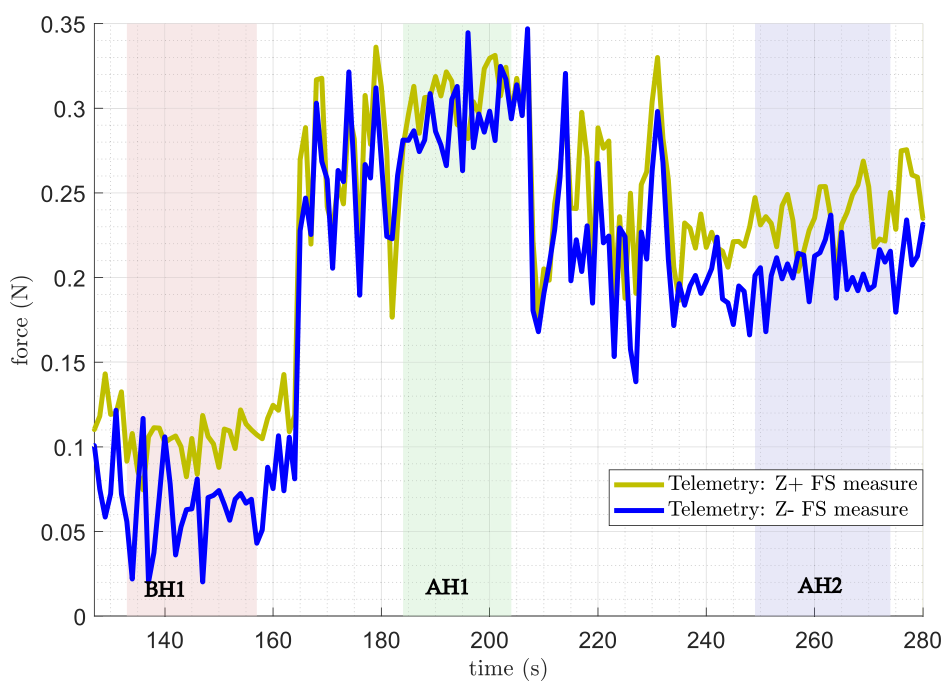

Fig. 14. Force signal recorded during the release test conducted on 29 June 2017, Test ID [0601] (TM1) as part of the LPF mission. The shaded intervals indicate the time periods used for the analysis of the fictitious force in the in-flight GPRM. Specifically, **BH1** (namely, *before handover 1*) corresponds to the interval before the Z^- handover, while **AH1** and **AH2** (namely, *after handover 1* and *2*) correspond to the intervals following the Z^- and Z^+ handovers, respectively.

tial force components, yielding the force differences at each stage, as expressed in the following three equations.

$$F_{Z^+} - F_{Z^-} = \begin{cases} (F_{n_2} - F_{n_1}) + (b_2 - b_1) & \text{for BH1} \\ (F_{n_2} - F_{n_1}) + (b_2 - b_1) - F_{f_1} & \text{for AH1} \\ (F_{n_2} - F_{n_1}) + (F_{f_2} - F_{f_1}) + (b_2 - b_1) & \text{for AH2} \end{cases} \quad (7)$$

Any noise contribution is reduced of about one order of magnitude by averaging the signals. The first fictitious force (F_{f_1}) can be obtained by the difference of the differential force ($F_{Z^+} - F_{Z^-}$) at BH1 and AH1 phases. Similarly, the second fictitious force (F_{f_2}) can be computed by the difference between the differential forces at AH2 and AH1. Since the observation time of F_{Z^+} and F_{Z^-} is the same across each phase, the bias contributions mutually cancel during the computation of their difference, making it possible to estimate the fictitious forces with a reasonable uncertainty.

$$\begin{cases} F_{f_1} = (F_{Z^+} - F_{Z^-})_{\text{BH1}} - (F_{Z^+} - F_{Z^-})_{\text{AH1}} \\ F_{f_2} = (F_{Z^+} - F_{Z^-})_{\text{AH2}} - (F_{Z^+} - F_{Z^-})_{\text{AH1}} \end{cases} \quad (8)$$

The Tables 2,3 present the mean values of the forces F_{Z^+} and F_{Z^-}, measured by the sensors, giving indication of the operative preload, before and after the analyzed handover. Then, they report the fictitious force value, estimated by Eq. 8, with its standard deviation.

The fictitious force in the Z^- GPRM (F_{f_1}) is approximately 20% of the value recorded for the LPF EQM GPRM, whereas at the Z^+ GPRM exhibits values ranging from 40% to 50% of those measured in the EQM GPRM.

The fictitious force acting on the two GPRM units (Z^- and Z^+) is estimated to lie in the range of approximately 0.02÷0.05N (see Table 2 and Table 3). As shown in Fig. 6, the majority of in-flight tests in which the applied preload force is comparable to the fictitious force exhibit a measurable delta displacement of the TM during the pre-release phase. Within this context, the in-flight GPRMs fictitious force (along with its associated uncertainty) serves as a threshold indicator for the detection of premature TM floating condition in the LPF releases.

5. Multi-body dynamic model of the GPRM in the presence of the control system

In this section, we introduce a multi-body model, built using MSC Adams, of the two GPRM units grabbing the TM, starting with insights into the design of the GPRM.

Table 2
The table presents the results of the analysis for the fictitious force components at the Z^- GPRM(TM1).

Test_ID	Mean F. BH1 (N)	Mean F. AH1 (N)	F_{f_1} (N)	STD. F_{f_1} (N)
0202	0.075	0.231	0.023	0.008
0502	0.249	0.274	0.025	0.007
0503	0.172	0.296	0.027	0.007
0601	0.086	0.303	0.028	0.009

Table 3
The table presents the results of the analysis for the fictitious force components at the Z^+ GPRM (TM1).

Test_ID	Mean F. AH1 (N)	Mean F. AH2 (N)	F_{f_2} (N)	STD. F_{f_2} (N)
0202	0.231	0.106	0.039	0.007
0502	0.274	0.305	0.035	0.006
0503	0.296	0.330	0.038	0.007
0601	0.303	0.237	0.043	0.007

The two GPRM units are modeled as depicted in Fig. 8b, with the floating TM placed in between the two.

As briefly described in the introduction, the plunger-linear runner assembly can be divided into 5 main components: the linear runner, the hollow plunger (the primary end effector), the force sensor, the tip, and the spacer, separating the piezo-stack actuator. At the front of the GPRM, the linear runner and the plunger are connected via a flex hinge. In the back, the linear runner is fixed to the force sensor. The tip is loaded with a spring against the front inner surface of the plunger. The tip is attached to the first piezo-stack of the stack unit. The second piezo stack is connected to the first trough a spacer, and is attached to the back of the plunger. The piezo stack actuators are commanded by an input voltage to move the release tip axially.

The nominal axial stiffness of the flex hinge is designed to be negligible with respect to the one of the force sensor. In this way, it can be considered as a prismatical joint, guiding the plunger at the front end of the runner.

To address the deformation of the plunger, it is modeled as two separate rigid bodies connected by a spring (K_{PL}). One of this bodies represent the plunger head (PL); the other one, is the plunger back (PL BK) and is body fixed to the force sensor hinge. The linear runner (LR), the tip (TP) and the spacer (SP) are modeled as rigid bodies. The flex hinge and the force sensor stiffness are modeled with two lumped springs at the front and the back of the runner (K_{FH} and K_{FS} respectively). The piezo are modeled as simple spring elements (K_{PZ}), with the electromechanical Bortoluzzi et al. (2011b); Zanoni and Bortoluzzi (2015) contribution embedded in the force F_{PZ}, in parallel to the spring elements.

The first axial mode of the Nexline actuator is approximated by the spring K_{NL}, between the linear runner and the ground. The motion commanded by the Nexline is modeled by stretching K_{NL} with a force.

A contact model for the interaction between plungers and TM, as well as between tip and TM, is introduced into the model. A detailed analysis of the adopted contact model can be found in (Tomasi et al., 2023).

The stiffnesses of the model components are estimated by independent finite element analysis or from components datasheets. However, for some components, the experimentally estimated stiffness were not compatible with the nominal values obtained from the FEM analysis. In particular, the parameters with the highest uncertainty are the stiffness of the flex hinge and of the washers spring, preloading the stack unit.

Eq. 9 reports the static free-body equations of the model, by considering the linear runner as ground.

$$\begin{cases} -K_{\mathrm{FS}} z_{\mathrm{FS}} - K_{\mathrm{PL}}(z_{\mathrm{FS}} - z_{\mathrm{PL}}) - K_{\mathrm{PZ}}(z_{\mathrm{FS}} - z_{\mathrm{SP}}) & = 0 \\ -K_{\mathrm{DS}}(z_{\mathrm{PL}} - z_{\mathrm{TP}}) - K_{\mathrm{FH}} z_{\mathrm{PL}} - K_{\mathrm{PL}}(z_{\mathrm{PL}} - z_{\mathrm{FS}}) & = 0 \\ -K_{\mathrm{PZ}}(z_{\mathrm{TP}} - z_{\mathrm{SP}}) - K_{\mathrm{DS}}(z_{\mathrm{TP}} - z_{\mathrm{PL}}) + F_{\mathrm{PZ}} - F_{\mathrm{TPTM}} & = 0 \\ -K_{\mathrm{PZ}}(z_{\mathrm{SP}} - z_{\mathrm{FS}}) - K_{\mathrm{PZ}}(z_{\mathrm{SP}} - z_{\mathrm{TP}}) - F_{\mathrm{PZ}} & = 0 \\ z_{\mathrm{TP}} = \delta_{\mathrm{tip}} \end{cases} \tag{9}$$

With the results reported in Table 1, some of the model parameters can be estimated by solving the system of Eqs. 9. Table 4 lists nominal values (from FEM analysis or components datasheets) and experimentally estimated values during EQM testing for selected model parameters.

5.1. GPRM Control System Implementation for Simulating the Test Mass Release Procedure

The model control system employs a co-simulation technique between MSC Adams and MATLAB Simulink. The nominal TM release procedure, implemented during LPF, is structured into four stages: grabbing, force relaxation, handover, and tip retraction. A TM release is considered nominal when the TM is released by the simultaneous retraction of the tips.

Fig. 15 schematizes the control system implemented in Simulink, resembling the flight control strategy. The control system gives the correct input to the model, and brings the model outputs as feedback. The LPF release procedure operates in rule-based control. Phases involving only the primary end-effector rely on contact-force feedback rather than instantaneous state of the end effector. Whereas in phases involving both end-effectors the control operates in open loop, these phases are terminated when the supply voltage of the secondary actuator (piezo stack) involved reaches its nominal value(120 Volts). A state machine is used to switch between the release procedure phases based on the conditions set on the model outputs. An independent control scheme is developed for each GPRM unit to reproduce in-flight operations.

- **Grabbing phase**: a constant velocity displacement is commanded to the linear runner. When the plungers get in contact with the runner, the force sensors start to measure a non-zero preload. The grabbing process ends when the measured force reaches the predefined threshold (2N in the case of LPF).
- **Force Relaxation phase**: the linear runner is gradually retracted, by producing a reduction of the pre-load, read by the force sensor. At the end of this phase, for LPF, the target pre-preload is 0.3N.
- **Handover phase**: both the tip and the linear runner are commanded simultaneously without feedback loop from force sensor. A ramp voltage is applied to one of the piezo stack, while a displacement command is issued to the Nexline in a coordinated way replicating the handover procedure performed in LPF. The handover is performed at the Z^{-} unit first, and then at the Z^{+} unit.
- **Tip retraction**: simultaneous shot down of the voltage signal applied to the piezo-stacks actuating the two tips. A retraction command is also sent to the linear runner to move away the plunger from the TM.

6. Simulation results of the TM release procedure and requirement identification

To gain deeper insight into the internal behavior of the GPRM during the release operation, as well as the interactions between the mechanism and the TM, simulations provide a valuable tool. In this subsection, we present the results obtained in the simulation, while reproducing a LPF test conducted during the extended mission.

6.1. Comparison between telemetry and simulation of anomalous in-flight releases

For the simulation, an in-flight case exhibiting floating TM during the pre-release phase is selected among the extended mission tests. Its handover is presented in Sec-

Table 4
Collection of a set of EQM (Z^{-}) stiffness parameters with their nominal values and the estimated ones, using the static equilibrium of the system with the extended tip and considering no mechanism preload. The stiffness of the Nexline is estimated by considering an global mechanism stiffness (tip-to-ground) in Z direction of 5.4×10^5N m^{-1}

Parameter	Nominal value		Estimated value		Units
	Value	Uncertainty	Value	Uncertainty	
K_{FS}	1.92×10^6	8×10^4	-		N m^{-1}
K_{PL}	2.21×10^7	9×10^5	-		
K_{PZ}	1.80×10^7	2×10^6	-		
K_{FH}	2.4×10^4	2×10^3	1.92×10^5	9×10^3	
K_{DS}	5.3×10^5	5×10^4	9.2×10^5	4×10^4	
K_{NL}	$\approx 4 \times 10^5$				

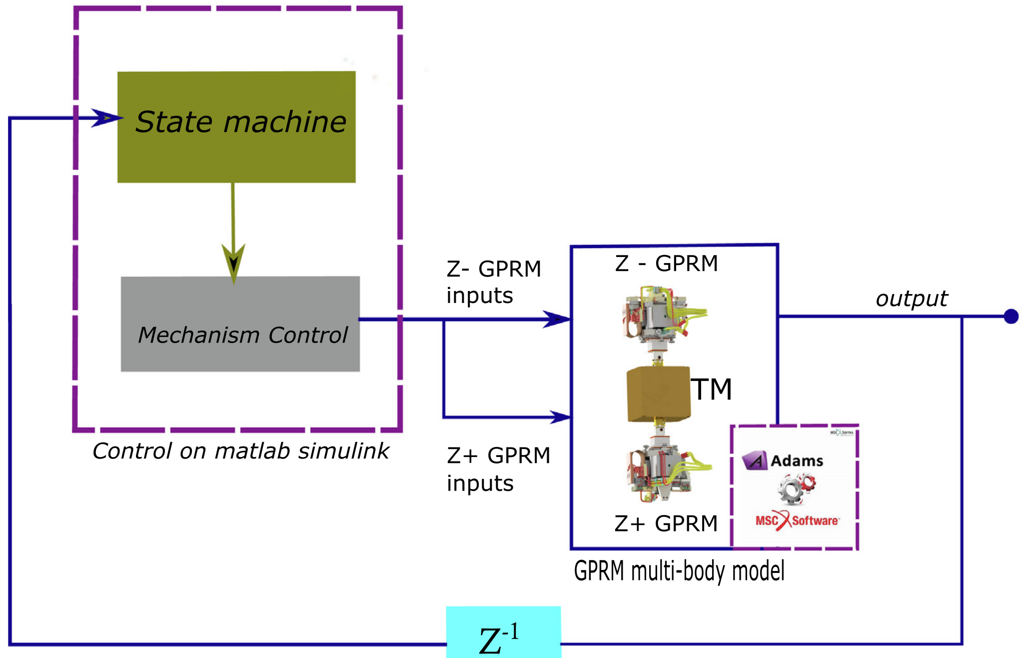

Fig. 15. Demonstration of a GPRM control system utilizing co-simulation techniques between MSC Adams and MATLAB Simulink. A state machine controls the mechanism operational phases to manage the TM release process. The output of MSC Adams is fed back to the state machine.

tion 3.2 (Fig. 8). Fig. 16 shows a comparison between the preload force measured at the Z^{-} and Z^{+} force sensor during in-flight operation and as a result from a multibody simulation.

In Fig. 16, the phases of the release are marked with numbers in the bottom part of the plot. The region before the first dashed line (1 in this case) corresponds to the grabbing phase. Phase (2) represents the idle state after TM is grabbed (post-grabbing), while phase (3) represents the force relaxation. After the reduction of the force, in time interval (4) the mechanism is in idle, waiting for the first handover (equivalently before Z^{-} handover (BH1)). The handover of the TM is performed twice: first by the Z^{-} (5) and then by the Z^{+} (7) GPRM unit.

Phase (6) illustrates an idle time between the two handovers. Intervals (8) and (9) represent the pre-release phases, with bias off and on respectively. It can be observed that the noise level increases when the bias is on (phase (9)). The state of the TM can be measured by the electrostatic sensing system only when the bias is on. The tip retraction

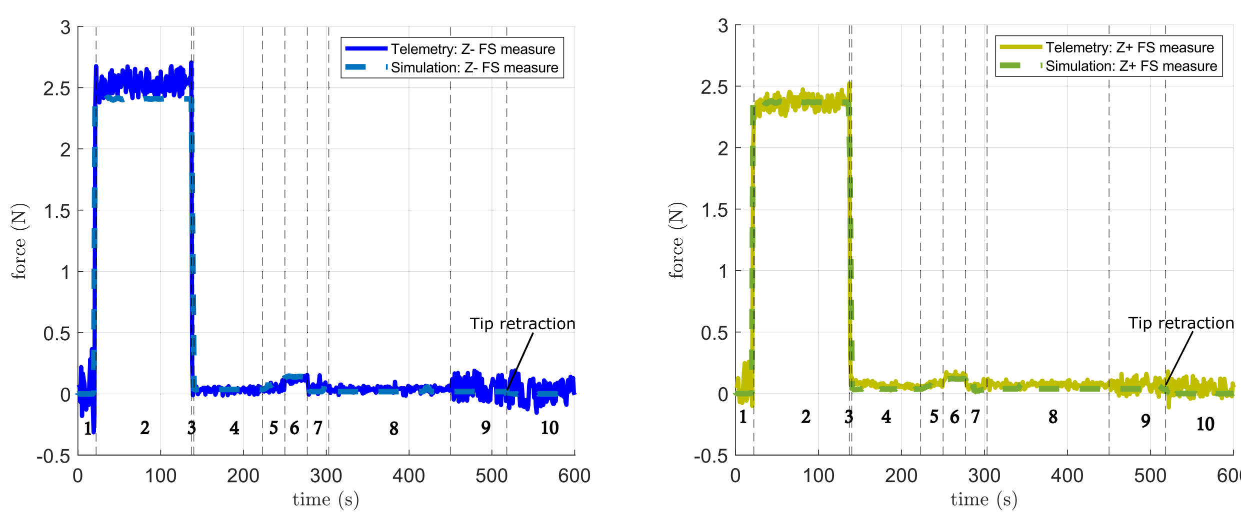

Fig. 16. In (a) and (b) the comparison of the measured force on the Z^{-} and Z^{+} GPRM is depicted respectively. The comparison is for a nominal release performed in-flight on 29 June 2017, Test ID [0302] (TM1) and with a simulation conducted using the multi-body dynamic model, developed in MSC Adams. This test exhibits a premature release in its pre-release phase, being associated to a non-zero delta displacement.

instant is also indicated in the figure. Phase (10) is after the retraction of the tip, where the two GPRM units are still and the TM is floating between them.

The simulated and measured plunger and tip displacements, with the comparison between the simulated contact force and telemetry force sensor data, are depicted in Fig. 17 for the Z^- and the Z^+ handover.

The most important insight from the simulation comes from the accessibility to all the components of the TM-GPRM force balance. In particular, the contact force between TM and plungers, and between landing areas and tips, as well as the force associated to the elastic deformation of the force sensor and the flex hinge.

In the GPRM static equilibrium, the contact force between the mechanism and the TM is equal to the sum of the forces in the force sensor (F_{FS}) and in the flex hinge (F_{FH}). Based on this observation, the force balance can be expressed as reported in Eq. 10, where F_{TPTM} and F_{PLTM} are the contact force between the TM and the tip or the plunger, respectively.

The simulation shows that there is a difference between the actual contact force and the force measured by the force sensor (see Fig. 18 and 19). This force difference is equal to the force required to deform the flex hinge.

$$F_{\mathrm{FH}} + F_{\mathrm{FS}} = F_{\mathrm{TPTM}} + F_{\mathrm{PLTM}} \tag{10}$$

Eq. 10 provides insight into the mechanism static equilibrium before the release phase of the simulated in-flight test.

During the handover procedure (see Fig. 17), the extension of the release tip and the retraction of the plunger is performed under open-loop control, without feedback from the force sensor to verify tip–TM contact. In the ini-

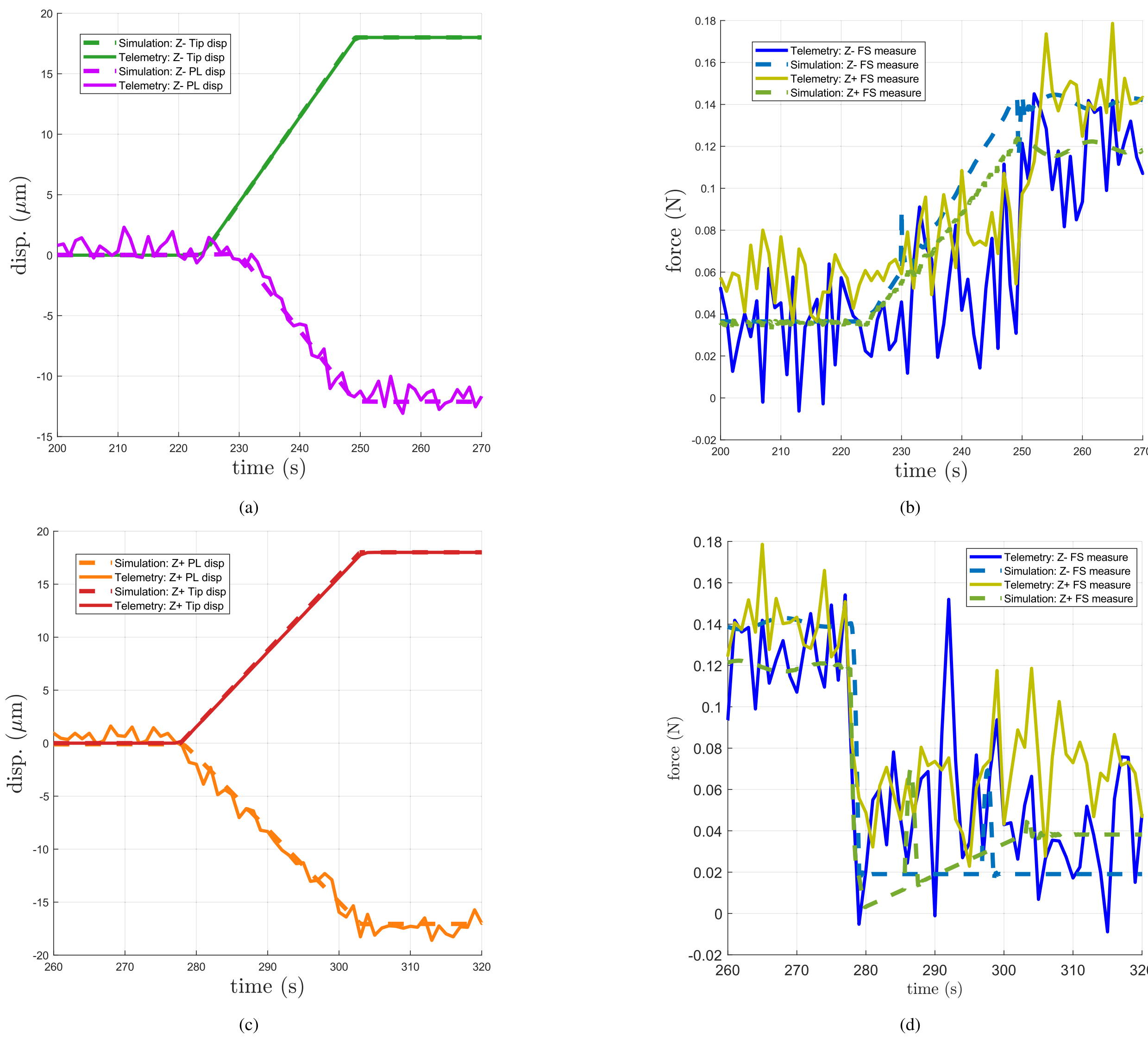

Fig. 17. The figure shows a focus of the handovers for the in-flight test performed on 29 June 2017, Test ID [0302] (TM1): the same shown in Fig. 16. (a) (c) show the displacements commanded to the release tip and plunger of the Z^- and Z^+ GPRMs during their respective handovers. When a handover to one unit is commanded, no motion is imposed to the unit not involved, i.e. the one at the opposite side of the TM. (b) and (d) show the forces measured by the force sensors. Each subfigure shows in-flight data compared .with simulation.

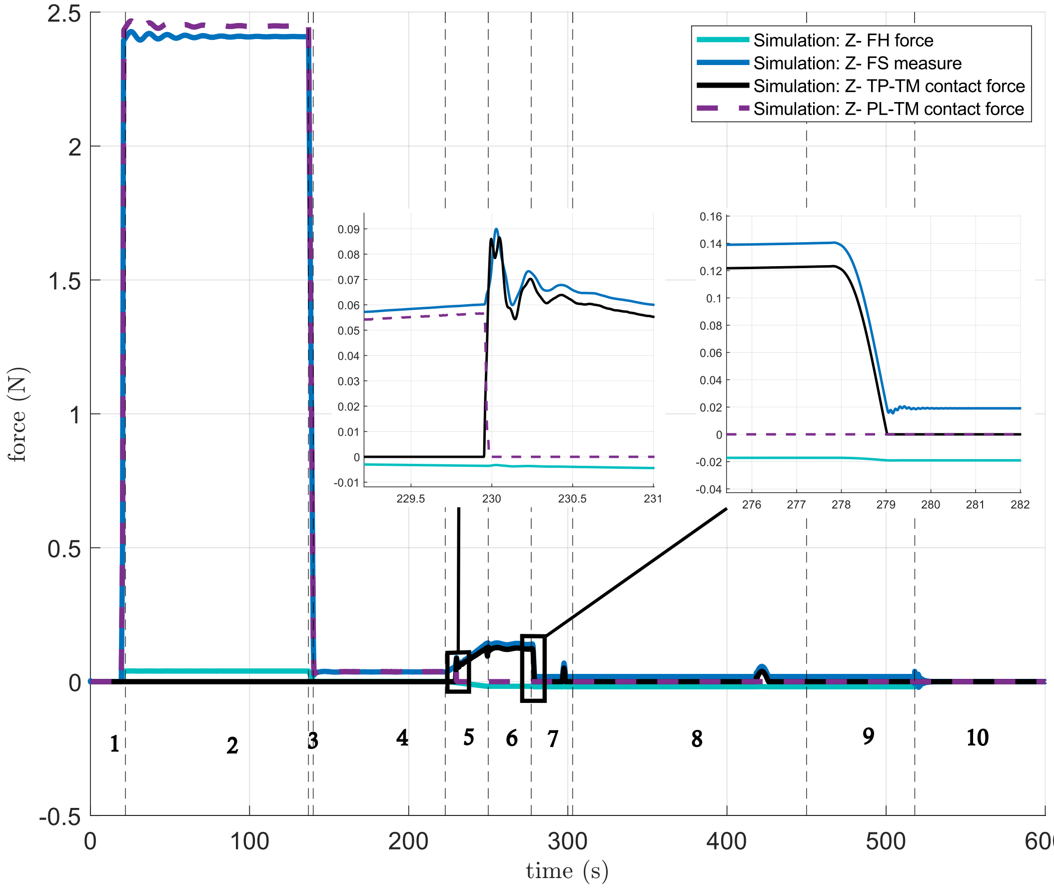

Fig. 18. The figure shows the internal dynamics of the Z^{-} GPRM during the release simulation of the in-flight release on 29 June 2017, Test ID [0302] (TM1). In the magnified box, the transition of TM contact from the plunger to the tip during the handover is shown. At the end of the Z^{-} handover, the TP-TM contact force is increased resulting from the extra displacement of the release tip relative to the plunger. During the Z^{+} handover, the tip–TM contact force is lost: the plunger–TM contact loss in the Z^{+} handover also causes the tip–TM contact in Z^{-} to be lost, compounded by the Z^{+} release tip failing to compensate for the intrinsic free stroke between the tip and the TM.

tial phase of the Z^{-} handover (Fig. 17a and 17b), the release tip extension was started and the plunger retraction was commanded when the tip reached approximately 4÷5μm, with a coordinated tip extension/plunger retraction.

This sequence facilitated the transfer of the holding function from the plunger to the release tip. A continuous increase in the measured force persists until the tip extension is complete. The delta force between the TP-TM contact force and the force recorded by the sensor is due to fictitious forces arising from the deformation of the plunger in response to the extension of the tip. This delta force corresponds to the fictitious force observed in the flight model.

The Z^{+} handover (Fig. 17c and 17d) is stared while Z^{-} tip and Z^{+} plunger are in contact with the TM. However, in the Z^{+} handover the release tip is extended and the plunger is retracted simultaneously, without the initial tip extension to recover the tip stroke. This sequence is present in all nominal Z^{+} handovers for LPF. This condition increases the likelihood of introducing a floating TM during the pre-release phase. According to the simulations, it is one of the causes of the observed delta displacements during in-flight tests under low-preload conditions (see Fig. 6).

However, in the cases the tip extension is faster than the plunger retraction, the tips can be anyway in contact with the LAs at the end of the handover, holding the TM.

The positive force observed in Figs. 18 and 19 (phase 8) in the force sensor, even when the actual contact force is zero, is due to fictitious forces arising from plunger deformation. The extended tip stretches the hollow plunger in between the force sensor and the flex hinge. Since no external forces are applied to the GPRM unit (no contact force), the force measured at the force sensor, i.e. the fictitious force, is perfectly balanced by the force in the flex hinge, deforming in the opposite direction (F_{FH} has negative sign - see Eq. 10).

6.2. Requirement identification to avoid premature release

The LPF GPRM is subject to a delta-development in view of the LISA. Among the proposed design improvements, the new version of the mechanism provides a longer stroke of the tip, to increase the nominal TM-plunger pre-

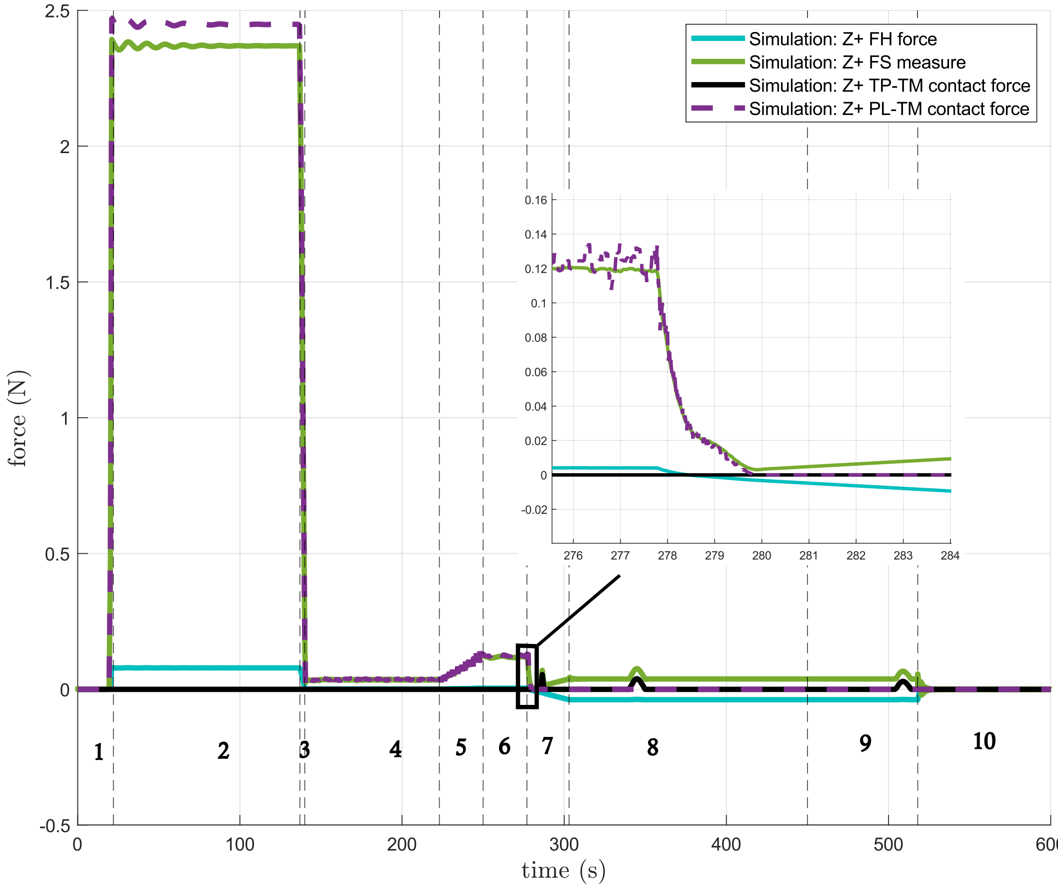

Fig. 19. The figure shows the internal dynamics of the Z^+ GPRM during the release simulation of the in-flight release on 29 June 2017, Test ID [0302] (TM1). As can be seen during the Z^+ handover, the contact force between the TM and the plunger is increased. This occurs because further extension of Z^- tip loads Z^+ force sensor through plunger TM contact in z^+ GPRM. During the z^+ handover, the z^+ plunger lose contact with the TM. This occurs because the release tip does not compensate for the free stroke that exists between the tip and the TM prior to the start of the z^+ handover. The z^+ force measure increases due to the fictitious force created during the free extension of the release tip. During the pre-release phase, there is no contact between the z^- or z^+ release tip and the TM.

release gap, preventing from recontact, and a less stiff force sensor, to improve its sensitivity (see (Zanoni et al., 2024)). These design changes on one side improve the performance of the mechanism but, on the other side, can worsen the effect of the fictitious force. For this reason, it is advisable to consider the presence of this interfering effect in the re-design of the mechanism. In this section, we derive a mechanical design requirement in order to limit the fictitious force. The static equations of the model reported in Fig. 13b make it possible to predict this effect as a function of the stiffnesses of the mechanism components, and of the tip stroke.

The static free-body equations, reported in Eq. 9, can be solved for z_{FS}, considering a tip extension $z_{TP} = \delta_{tip}$. Considering the case of no preload applied to the mechanism ($F_{TPTM} = 0$), the force in the force sensor ($F_{\mathrm{FS}} = -K_{\mathrm{FS}} z_{\mathrm{FS}}$) is equal to the fictitious force (F_f). The result is reported in Eq. 11. A requirement can be set on the parameters contributing to the fictitious force value, constraining it to be lower than a threshold value (γ), compatible with the noise.

$$F_{\mathrm{FS}}|_{F_{TMTP}=0} = F_f = \frac{K_{DS} K_{FH} K_{FS}}{K_{DS} K_{FS} + K_{FH} K_{FS} + K_{FH} K_{PL} + K_{FS} K_{PL}} \delta_{tip} < \gamma \tag{11}$$

The GPRM delta-development performed in view of LISA brings to a marginal modification of both plunger and force sensor, affecting their stiffness (see Table 5). Moreover, the longer tip stoke negatively affect the fictitious force effect. By using the requirement reported in Eq. 11,

Table 5
Data for the GPRM components as a result of the GPRM delta development in view of LISA. The last row reports the maximum value of the flex-hinge stiffness which gives fictitious force value lower than γ.

Parameter	Value	Unit
K_{FS}	6.59×10^5	N m^{-1}
K_{PL}	1.95×10^7	N m^{-1}
K_{DS}	5.3×10^5	N m^{-1}
δ_{tip}	27	μm
γ	0.02	N
$K_{FH,\max}$	2.92×10^4	N m^{-1}

the effects of the updated parameters can be evaluated. By inverting the equation, we can set the maximum value in the stiffness of the flex-hinge ($K_{FH,\max}$), bringing to a negligible value of fictitious force ($\gamma = 0.02$N as for the in-flight Z^- unit, of sensor 1). The result is reported in Table 5.

In addition, we also suggest to calibrate eventual residual fictitious force effects, to compensate for them via software and have a more reliable diagnostic on the TM preload in pre-release.

7. Conclusion

In this work the operations of the LISA Pathfinder GPRM, functional to the TM release, have been analyzed and simulated. The results indicate that, for low preload force, loss of contact between the tip and the TM occurred during the pre-release phase, leading to a premature and uncontrolled TM release, highlighted by significant delta displacements. Some root causes of the anomalous prerelase behavior are identified.

1. A TM grabbed configuration characterized by large rotations and limited co-penetration of the plungers in their indents. This produces a large tip-LA clearance, limiting the effectiveness of the tip extension and the realization of an effective contact.
2. The implementation of an open-loop control strategy in the handover procedure, which relies on the synchronization of the tip and plunger opposite motion to shift the mechanism-TM mechanical interface from the plunger to the tip. In particular, the method used during the Z^+ handover, in which the plunger is commanded from the beginning, may lead to the absence of contact in prerelease condition (before the tip retraction).
3. The generation of a fictitious force signal produced by the free extension of the tip. This limits the possibility to check the mechanism/TM state before release, potentially leading to a false tip-TM contact detection.

Furthermore, the force sensor exhibited excessive noise during the activation of the plunger bias, with amplitudes comparable with the low preload force applied in prerelease. These anomalies in the release mechanism may lead to an unconstrained TM prior to the nominal release, increasing the risk of TM–plunger re-contact and resulting in a noncompliant TM velocity at the release.

For the forthcoming LISA mission, we recommend to design the GPRM, focusing also on the handover procedure, in order to guarantee a permanent TM handling over the overall release procedure. The advantages and limitations of the open-loop handover strategy used for LISA Pathfinder require an in-depth evaluation through dedicated ground tests. We recommend to involve the force signal in the control loop during handover procedure, but taking into account the effects of a fictitious force signal, if non-perfectly compensated by design. To ensure a successful release, the TM position and attitude signals may be monitored prior to the tip retraction as a confirmation of TM stability. Additionally, the plunger co-penetration can be another important index of a successful grabbing, bringing to safer following operations. Finally, limiting the force sensor noise is essential to improve the control of the release process.

Addressing the key issues identified in the release mechanism is critical to ensure the reliable and precise operation required to meet the strict LISA requirements. These findings highlight the importance of refining the TM release strategy, for having more reliable grabbing and handover, paving the way to successful TM releases for LISA.

Declaration

Declaration of generative AI and AI-assisted technologies in the manuscript preparation process. During the preparation of this work the authors used ChatGPT in order to Improving English or grammar. After using this tool/service, the authors reviewed and edited the content as needed and takes full responsibility for the content of the published article.

Declaration of competing interest

The authors declare the following financial interests/personal relationships which may be considered as potential competing interests:Abaraham Ayele Gelan reports financial support was provided by Italian Space Agency. If there are other authors, they declare that they have no known competing financial interests or personal relationships that could have appeared to influence the work reported in this paper.

Acknowledgments

This work has been made possible by the LISA Pathfinder mission, which is part of the space-science program of the European Space Agency, and has been supported by Istituto Nazionale di Fisica Nucleare (INFN) and Agenzia Spaziale Italiana (ASI), with a fund Decreto Ministeriale $\mathcal{N}^{\underline{o}}$ 352 del 09/04/2022.

References

Amaro-Seoane, P., Audley, H., Babak, S. et al., 2017. Laser interferometer space antenna. https://arxiv.org/abs/1702.00786. arXiv:1702.00786.

Armano, M., Audley, H., Auger, G., et al., 2016. Sub-femto-g free fall for space-based gravitational wave observatories: Lisa pathfinder results. Phys. Rev. Lett. 116, 231101. https://doi.org/10.1103/PhysRevLett.116.231101, URL: https://link.aps.org/doi/10.1103/PhysRevLett.116.231101.

Armano, M., Audley, H., Baird, J., et al., 2018. Beyond the required lisa free-fall performance: New lisa pathfinder results down to 20μHz. Phys. Rev. Lett. 120, 061101. https://doi.org/10.1103/PhysRevLett.120.061101, URL: https://link.aps.org/doi/10.1103/PhysRevLett.120.061101.

Bell, T.E., 2008. Hearing the heavens: the cosmos is thought to be awash with gravitational waves to which humanity is, as yet, deaf. trudy e. bell reports on lisa, an experiment on an unprecedented scale designed to put that right. Nature 452 (7183), 18–22.

Benedetti, M., Bortoluzzi, D., Vitale, S., 2008. A momentum transfer measurement technique between contacting free-falling bodies in the presence of adhesion. J. Appl. Mech. 75 (1), 011016. https://doi.org/10.1115/1.2755104, arXiv:https://asmedigitalcollection.asme.org/appliedmechanics/article-pdf/75/1/011016/5476334/011016_1.pdf.

Bortoluzzi, D., Baglivo, L., Benedetti, M., et al., 2009. Lisa pathfinder test mass injection in geodesic motion: status of the on-ground testing. Class. Quantum Gravity 26 (9), 094011. https://doi.org/10.1088/0264-9381/26/9/094011.

Bortoluzzi, D., Benedetti, M., Baglivo, L., et al., 2011a. Measurement of momentum transfer due to adhesive forces: on-ground testing of in-space body injection into geodesic motion. Rev. Sci. Instrum. 82 (12), 125107. https://doi.org/10.1063/1.3658479.

Bortoluzzi, D., Conklin, J.W., Zanoni, C., 2013. Prediction of the LISA-Pathfinder release mechanism in-flight performance. Adv. Space Res. 51 (7), 1145–1156, Https://doi.org/10.1016/j.asr.2012.11.001.

Bortoluzzi, D., Foulon, B., Marirrodriga, C.G., et al., 2010. Object injection in geodesic conditions: in-flight and on-ground testing issues. Adv. Space Res. 45 (11), 1358–1379.

Bortoluzzi, D., Mäusli, P.A., Antonello, R., et al., 2011b. Modeling and identification of an electro-mechanical system: the LISA grabbing positioning and release mechanism case. Adv. Space Res. 47 (3), 453–465.

Bortoluzzi, D., Vignotto, D., Dalla Ricca, E., et al., 2021a. Investigation of the in-flight anomalies of the LISA Pathfinder test mass release mechanism. Adv. Space Res. 68 (6), 2600–2615.

Bortoluzzi, D., Vignotto, D., Zambotti, A., et al., 2021b. In-flight testing of the injection of the lisa pathfinder test mass into a geodesic. Adv. Space Res. 67 (1), 504–520.

Conklin, J., Apple, S., Álvarez, A. et al., 2025. Grattis: the gravitational reference advanced technology test in space. (p. 79). doi:10.1117/12.3061925.

Dalla Ricca, E., Bortoluzzi, D., Vignotto, D., 2025. Analysis and interpretation of the in-flight dynamics of a critical space mechanism. Adv. Space Res. 75 (1), 542–559.

Dalla Ricca, E., Bortoluzzi, D., Zanoni, C., 2024. An improved vibration multi mode-based technique for the characterization of metallic adhesion impulses. AIAA J. 62 (10), 3988–3998.

Dolesi, R., Bortoluzzi, D., Bosetti, P., et al., 2003. Gravitational sensor for LISA and its technology demonstration mission. Class. Quantum Gravity 20 (10), S99.

Dávila Álvarez, A., Knudtson, A., Patel, U., et al., 2022. A simplified gravitational reference sensor for satellite geodesy. J. Geodesy 96 (10). https://doi.org/10.1007/s00190-022-01659-0.

Footdale, J., Sypolt, C., Mackin, J., et al., 2024. Caging and release mechanism design for the simplified gravitational reference sensor. In: Proceedings of the 47th Aerospace Mechanisms Symposium (pp. 1–14). NASA Langley Research Center, Hampton, VA, pp. 1–14. Available: https://www.esmats.eu/amspapers/pastpapers/pdfs/2024/footdale.pdf.

Grimm, C.D., Grundmann, J.-T., Hendrikse, J. et al., 2019. From idea to flight - a review of the mobile asteroid surface scout (mascot) development and a comparison to historical fast-paced space programs. Progress in Aerospace Sciences, 104, 20–39. URL: https://www.sciencedirect.com/science/article/pii/S0376042118301222. doi: 10.1016/j.paerosci.2018.11.001.

Grimm, C.D., Lange, C., Lange, M., et al., 2020. The mascot separation mechanism. CEAS Space Journal 12, 343–365, URL: https://api.semanticscholar.org/CorpusID:255607335.

Koker, I., Rozemeijer, H., Stary, F. et al., 2013. Alignment and testing of the gprm as part of the ltp caging mechanism. In Proceedings 15th European Space Mechanisms and Tribology Symposium (ESMATS) (p. 21). volume 718.

Mäusli, P., Romano, R., Lips, K. et al., 2007. GPRM-Design description. ESA internal document S2-HTS-DDD-3001, ESA.

McNamara, P., Vitale, S., Danzmann, K., et al., 2008. Lisa pathfinder. Class. Quantum Gravity 25 (11), 114034. https://doi.org/10.1088/0264-9381/25/11/114034.

Montemurro, F., Fichter, W., Schlotterer, M., et al., 2006. Control design of the test mass release mode for the lisa pathfinder mission. AIP Conf. Proc. 873 (1), 583–587. https://doi.org/10.1063/1.2405103, arXiv: https://pubs.aip.org/aip/acp/article-pdf/873/1/583/11790499/583_1_online.pdf.

Schleicher, A., Ziegler, T., Schubert, R., et al., 2018. In-orbit performance of the lisa pathfinder drag-free and attitude control system. CEAS Space Journal 10, 471–485.

Tomasi, M., Dalla Ricca, E., Vignotto, D. et al., 2023. Development of a dynamical model of a release mechanism for in-flight performance prediction. Advances in Space Research, 72(11), 4950–4964. URL: https://www.sciencedirect.com/science/article/pii/S0273117723007445. doi: 10.1016/j.asr.2023.09.022.

Tomasi, M., Dalla Ricca, E., Vignotto, D. et al. (14th LISA Symposium, Dublin, 2022). Analysis of the grabbing positioning and release mechanism performance sensitivity to alignment.

Vignotto, D., 2021. Analysis of the In-Flight Performance of a Critical Space Mechanism. In: Ph.D. thesis Doctorial School in Matherials, Mechatronics and Systems Engineering.

Vignotto, D., Zanoni, C., Tomasi, M., et al., 2023. The role of friction in the lisa-pathfinder release mechanism anomaly. AIAA J. 61 (12), 5232–5241.

Wanner, G., 2019. Space-based gravitational wave detection and how lisa pathfinder successfully paved the way. Nat. Phys. 15 (3), 200–202.

Zahnd, B., Zimmermann, M., Spörri, R., 2013. Lisa-pathfinder cage and vent mechanism-development and qualification. In: Proceedings 15th European Space Mechanism and Tribology Symposium (ESMATS), pp. 1–7.

Zanoni, C., Bortoluzzi, D., 2015. Experimental-analytical qualification of a piezoelectric mechanism for a critical space application. IEEE/ASME Trans. Mechatron. 20 (1), 427–437. https://doi.org/10.1109/TMECH.2014.2333057.

Zanoni, C., Bortoluzzi, D., Vignotto, D., et al., 2024. Development plan of the upgraded release mechanism for the LISA space mission. In: AMS Space Mechanisms Symposium.